(THIS PAGE INTENTIONALLY LEFT BLANK)

AN ABSTRACT OF THE THESIS OF

Nicholas C. Wilson for the degree of Master of Science in Civil Engineering presented on May 22, 2017.

Title: Radiometric Calibration of EAARL-B Bathymetric Lidar Data.

Abstract approved: _____

Christopher E. Parrish

The Experimental Advanced Airborne Research Lidar - B (EAARL-B), which was built and deployed by the U.S. Geological Survey (USGS) in 2014, is a novel topographic-bathymetric lidar system. While retaining a number of features that were pioneered in the original National Aeronautics and Space Administration (NASA) EAARL system (e.g., low energy, short pulse width, narrow receiver field of view, green-only laser wavelength), the EAARL-B added a split-beam, four-channel design to improve bathymetric data density and depth measurement range (up to 44 m in clear water). In 2014, the EAARL-B was used to acquire bathymetric data in the U.S. Virgin Islands (USVI), in support of the National Oceanic and Atmospheric Administration (NOAA) Center for Coastal Monitoring and Assessment (CCMA) Biogeography Branch. The enhanced capabilities of the EAARL-B system, combined with updated algorithms in the processing software, provided high-quality data covering over 600 km^2 in the USVI, filling critical data gaps. However, the EAARL-B processing software and workflows were lacking a set of tools and procedures to exploit return waveforms (digitized samples of the backscattered signal) for generating seafloor reflectance mosaics and characterizing seafloor composition. This functionality is of significant interest to CCMA to support benthic habitat mapping and management of coral reef ecosystems. While seafloor reflectance mapping and waveform feature extraction tools do exist, in varying degrees and forms, for other bathymetric lidar systems, the extension of these capabilities to the EAARL-B is challenging, due to the system's unique design. The goal of this study was to address this need, through development and testing of a new set of processing procedures and algorithms for generating seafloor relative reflectance mosaics and gridded waveform features from EAARL-B data. The procedures were developed using data from two test sites: Barnegat Bay, New Jersey, and Buck Island, north of Saint Croix. After testing and refining the methods, a seafloor relative reflectance mosaic was generated for a large site south of Saint

Thomas. Additionally, raster grids of waveform shape features were produced for a smaller study site encompassing Flat Cays, south of Charlotte Amalie, Saint Thomas. The procedures have been demonstrated to enable generation of seamless seafloor data products, in which the effects of confounding variables, such as depth, incidence angle, and flight direction, have been virtually eliminated. Current research, led by project partners at NOAA CCMA and the University of New Hampshire, is focusing on using the results of this work to predict species richness, canopy cover, complexity, and coral health (including disease and bleaching) and other parameters for the USVI project sites.

Radiometric Calibration of EAARL-B Bathymetric Lidar Data

by
Nicholas C. Wilson

A THESIS

submitted to

Oregon State University

in partial fulfillment of
the requirements for the
degree of

Master of Science

Presented May 22, 2017
Commencement June 2017

Master of Science thesis of Nicholas C. Wilson presented on May 22, 2017.

APPROVED:

Major Professor, representing Civil Engineering

Head of the School of Civil and Construction Engineering

Dean of the Graduate School

I understand that my thesis will become part of the permanent collection of Oregon State University libraries. My signature below authorizes release of my thesis to any reader upon request.

Nicholas C. Wilson, Author

ACKNOWLEDGEMENTS

I would first like to thank my advisor Chris Parrish for your guidance and assistance throughout my time as a graduate student at OSU. This work would truly not be possible without your support.

I would also like to thank my committee members Michael Olsen, Merrick Haller and Jamon Van Den Hoek for their time and efforts put forth in reviewing and providing feedback on this thesis.

Thank you to Dan Gillins and Mike Eddy, for without your consideration, graduate school would not be a possibility for me.

Thank you to Tim Battista, Bryan Costa, Wayne Wright, David Nagle, Christine Kranenburg, and Jenn Dijkstra for your involvement in various aspects of this research. This appreciation extends to NOAA NCCOS CCMA for making this research possible.

Finally I would like to thank my family and friends supporting me in my decision to extend my academic career.

TABLE OF CONTENTS

Page

TABLE OF CONTENTS (Continued)

Page

LIST OF FIGURES

Figure Page

LIST OF FIGURES (Continued)

Figure Page

1. INTRODUCTION

1.1 Benthic Habitat Mapping

Benthic habitat maps, which depict the spatial extents and distributions of coral reefs and other seafloor habitats, are valuable to coastal management offices and policy makers in managing coastal ecosystems and assessing changes over time (Mumby & Harbone, 1999; Costa et al., 2009 (a); Brown et al., 2011). For example, benthic habitat maps can help inform policy decisions related to the placement or modification of marine protected areas (MPAs) and the prioritization of areas for further study (Monaco et al., 2012). Coral reef ecosystems are particularly vulnerable to environmental stressors, leading to a need to accurately delineate coral reef boundaries such that change can be assessed, and management decisions can be made. In the U.S. Virgin Islands (USVI), coral reefs provide a range of ecosystem services, from shoreline protection to fishing and tourism, but are currently in a state of decline (Catanzaro et al., 2002; Jeffrey et al., 2005; Rothenberger et al., 2008).

Since 2000, the National Oceanic and Atmospheric Administration (NOAA) has been charged with leading federal efforts to generate comprehensive habitat maps of all U.S. shallow-water coral reef ecosystems (Monaco et al., 2012). Within NOAA, the National Ocean Service (NOS), National Centers for Coastal Ocean Science (NCCOS), Center for Coastal Monitoring and Assessment (CCMA) Biogeography Branch is actively involved in conducting biogeographic assessments and producing habitat maps. The production and management of a large suite of habitat maps necessitates ongoing research into new mapping tools and techniques (Costa et al., 2009 (a); Pittman & Brown, 2011; Brown et al., 2011).

1.2 Seafloor Composition Mapping Technologies

Mapping seafloor composition is inherently difficult for a number of reasons. Direct, *in situ* observation and measurement (for example, by divers), is generally infeasible, due to the amount of time it would take to map even a moderately-sized area. In addition to the expense, diving can be logistically challenging and even dangerous in a number of areas. Therefore, shipborne, airborne, and spaceborne remote sensing technologies, such as airborne bathymetric lidar, multibeam echosounding (MBES), hyperspectral imaging, aerial photography, and satellite imaging provide the most practical means of seafloor mapping over large spatial extents. While acoustic techniques (i.e., sonar) are most effective in deeper water, bathymetric or topographic-bathymetric lidar is often an effective and cost-efficient technology for mapping nearshore bathymetry.

Airborne lidar and multibeam sonar are two commonly compared bathymetric mapping techniques. In some projects, the cost of mapping with airborne lidar can be between one fifth and one half of mapping the same region with sonar (Guenther et al 2000). This is primarily due to the increased speed that a plane can travel, and wider swath width. Airborne lidar also has the advantage in very shallow, near-shore regions in which it would be unsafe to collect data on a boat (Guenther et al., 2000). Many bathymetric lidar systems also have the capability to map topography, allowing seamless topo-bathy products to be created.

While airborne lidar is advantageous in shallow regions, multibeam sonar can be used under much deeper conditions, and at a higher resolution. Both techniques have a measurable backscatter, or "intensity," value associated with the return signal. The surface characteristic information that can be inferred from each signal return amplitude differs (Costa et al., 2009 (a)). Where multibeam backscatter gives information about the hardness of the surface, the lidar peak bottom return amplitude gives information about the reflectivity of the surface at the laser wavelength. Because both of these techniques have unique advantages in the environment they can collect in, the information about surface characteristics they can provide, it important to plan missions accordingly to ensure the appropriate sensor—or combination of sensors—is selected.

Lidar utilizes the two-way travel time of an emitted laser pulse, based on the knowledge of the speed of light through air and/or water to calculate ranges. These ranges are combined with post-processed position and orientation data from a GNSS-aided inertial navigation system (INS), scan angles, and other data to produce *X, Y, Z* point clouds. Recording a time-series of return pulse amplitude, along with the use of a green laser (532 nm wavelength) allows bathymetric lidar systems the capability of calculating depth values in shallow water environments. Figure 1-1 shows an idealized bathymetric lidar return waveform. This waveform can be broken down into three components. The water surface return provides information about the pulse interaction with the water surface. Water column backscattering results from a portion of the incident pulse being scattered back in the direction of the receiver from particulate matter in the water column as the pulse travels through the water. Exponential attenuation of the downwelling irradiance also occurs within the water column. The bottom return, which can be obscured by the water column backscatter in deep water or in low reflectivity situations, is the portion of the return signal corresponding to the interaction of the pulse with the seafloor.

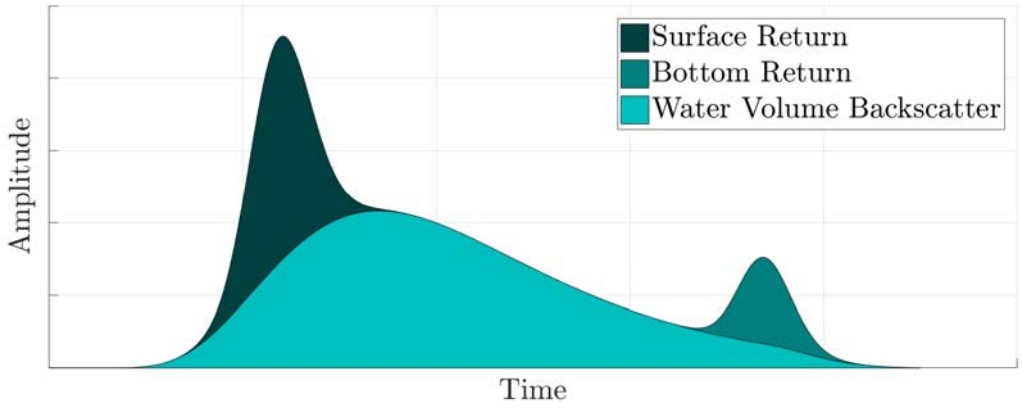

Figure 1-1: Idealized bathymetric lidar return waveform (adapted from Wang & Philpot 2006 and Gary Guenther)

The seafloor characteristics that can be derived from the bathymetric lidar waveform extend beyond depth. Bathymetric lidar data provides information about the structure of the seafloor. Together with products generated from bathymetry such as slope, rugosity and curvature, the seafloor morphology can be characterized. Additional metrics generated from the shape of bathymetric lidar returns, such as peak amplitude, area under the curve, skewness, and standard deviation, have the potential of assisting in benthic habitat characterization (Collin et al., 2011). Before the utility of these metrics can be assessed, artifacts which can dominate the return waveform must be accounted for.

Correction and processing procedures are needed to prepare the bottom return peak amplitude values to be used as input to an object-oriented classification procedure for producing benthic habitat maps. While, the amplitude of the bottom return contains information related to seafloor reflectance, unfortunately, there are a number of systematic and environmental factors that influence the shape of the waveform. Figure 1-2 illustrates the collection geometry of bathymetric lidar and how the pulse interacts with its environment throughout the scanning process.

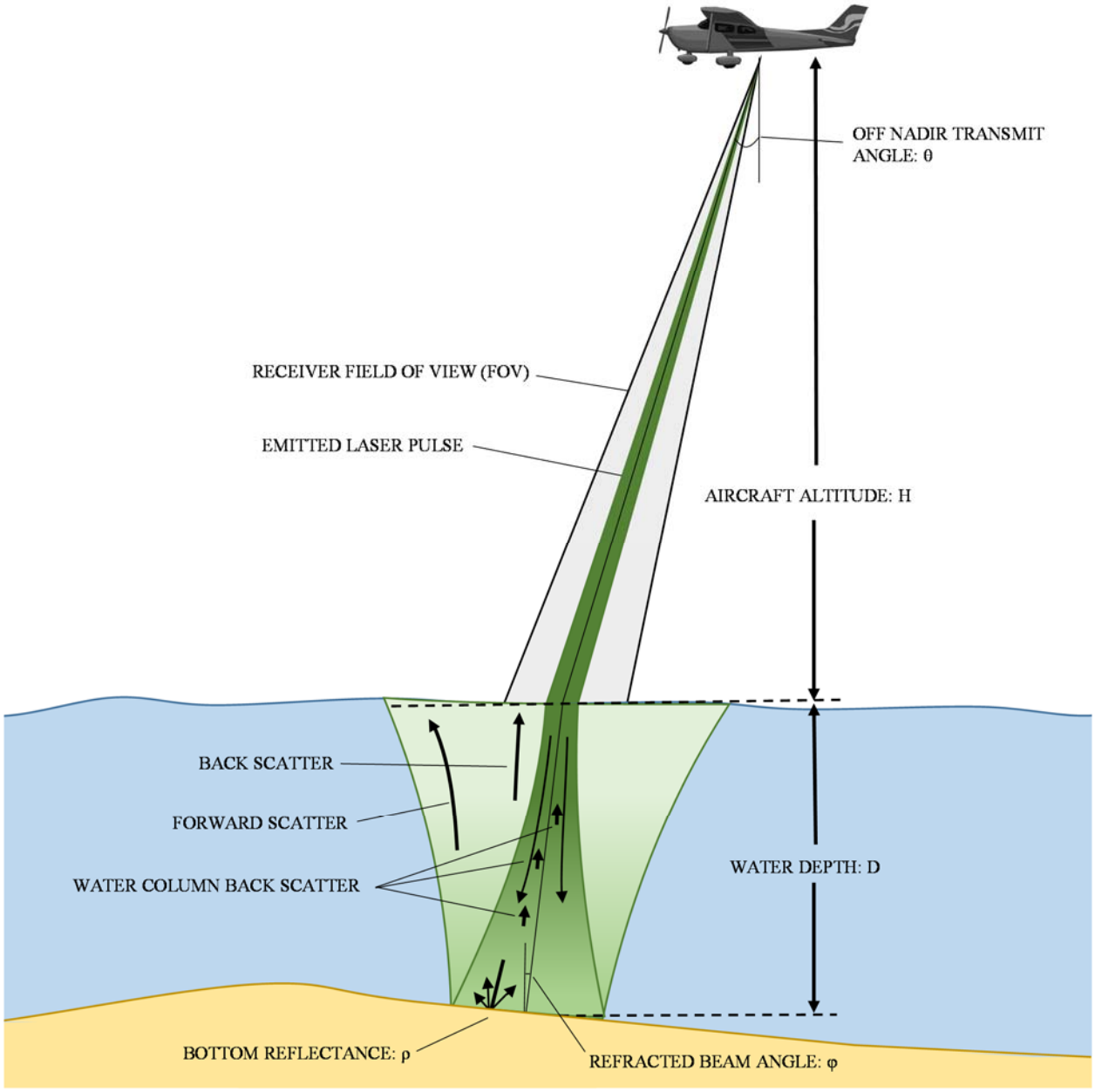

Figure 1-2: Typical bathymetric lidar acquisition geometry (Kashani et al., 2015).

The dominant factors affecting amplitude are scattering and absorption within the water column, which cause the amplitude to decay exponentially at a rate associated with the clarity of the water and laser wavelength (typically, 532 nm for bathymetric lidar). The angle at which the incident pulse interacts with the seafloor surface also significantly impacts the shape of the bottom return, due to specular components of the bottom reflectance and pulse stretching (Wang and Philpot, 2002). Rigorous correction of the received signal to yield true seafloor reflectance requires extensive knowledge of the

system used to collect the data, and the environment the data were collected, both of which may not be available. As a practical alternative to true seafloor reflectance, so-called “relative reflectance” provides an arbitrarily-scaled measure of a location’s brightness relative to other locations on the surface in arbitrary units of digital numbers (DN) (e.g., 0-255 for an 8-bit relative reflectance image). Relative reflectance mosaics can provide valuable information for applications in which knowledge of seafloor composition is important.

1.3 EAARL-B Overview

The topo-bathy lidar system focused on in this work is the Experimental Advanced Airborne Research Lidar - B (EAARL-B), developed by C. Wayne Wright at the U.S. Geological Survey (USGS) and pictured in Figure 1-3. Compared to the first edition EAARL system, the EAARL-B features an increased point density due to the emitted laser pulse being split into three pulses. Depth capabilities were also enhanced from approximately 27 meters to 44 meters by increasing the total peak laser power by a factor of 10, and by including a deep-water, wider field of view (FOV) receiver channel (Wright et al., 2016).

The EAARL-B system differs from other commonly used topo-bathymetric lidar system in a number of ways, including its small receiver field of view, scan geometry and transmit power. Quandros (2013) provide an organized figure outlining differences in bathymetric lidar sensor specifications. These differing system designs and specifications affect the measurement capabilities of the systems (e.g., minimum and maximum depth measurement capabilities, point densities, and accuracies) and also affect the types of corrections that may need to be applied to return waveforms.

Figure 1-3: Mounted EAARL-B System (image courtesy of C. Wayne Wright).

The three incident laser pulses reach the water surface with nominal diameter of 30 cm at the typical flight altitude of 300 meters. Each spot has a corresponding receiver channel with an approximate field of regard of 60 cm (diameter). The deep-water receiver channel is designed to encompass all of the shallow-water specific channels and views a 5-m diameter region at the water surface. The narrow receiver FOV for the shallow channels follows the pioneering design of the original EAARL system, which represented a design departure from conventional bathymetric lidar systems that used much wider receiver FOVs (Feygels et al., 2003 (a)). As incident light is either scattered or absorbed by particulate matter in the water column, receiver size is (in conventional bathymetric lidar systems) more commonly kept large to increase the likelihood that a return pulse will be detected, and, therefore, increase the maximum depth measurement capability.

Post-processing of data collected with the EAARL-B is done in the Airborne Lidar Processing System (ALPS). This software analyzes the lidar return waveform, aircraft position and orientation data to produce a point cloud of the target surface. Waveform analysis is performed through three different surface detection methods. Each detection method is designed for a specific surface type, such as unvegetated topography, vegetated topography, and submerged topography (i.e., bathymetry) (Nagle & Wright, 2016).

For the shallow receiver water channels' waveforms, the water column backscatter is modeled by fitting an exponential decay function to the waveform. For deep water receiver channels, the water column backscatter is modeled by fitting a log-normal function to the waveform. Different backscatter removal algorithms are needed for the system because of optical differences in the design of the deep and shallow channels. A detailed description of waveform processing algorithms with pseudocode can be found in Nagle & Wright (2016).

1.4 Previous USVI Mapping Projects

Past habitat mapping efforts in the U.S. Virgin Islands have utilized multiple data sources to delineate habitat types. Early work to create the first shallow-water coral reef inventory relied on visual interpretation of orthorectified aerial photographs acquired in 1999. This work resulted in the creation of the Habitat Digitizer ArcView extension, a tool which allows for hierarchical classification schemes to be created and for habitat polygons to be rapidly delineated (Kendall et al. 2001). This work covered a large area, but was limited by: 1) the use of visual interpretation, which involves some level of subjectivity and can limit the repeatability of the results, and 2) the limited depth range associated with passive remote sensing methods.

From 2008 to 2009, benthic habitat maps for shallow depth (<30 m) and moderate depth (30-60 m) regions were generated for areas surrounding St. John (Zitello et al., 2009 and Costa et al., 2009 (b)). Shallow depth mapping utilized techniques consistent with Kendall et al. 2001. Aerial and satellite imagery were used to visually interpret habitat classifications. This served as an improvement over past efforts in that the classification scheme was enhanced, and the minimum mapping unit (MMU) was reduced. Moderate depth regions were mapped using acoustic backscatter data from a multi-beam echosounder. Metrics derived from depth information given by the sonar, along with the intensity of returns, were used to delineate habitat types using a semi-automated approach. This approach involved

an edge detection algorithm, which removed the subjectivity of edges being delineated by visual interpretation. This new approach also proved to produce results seven times more time efficiently than past methods (Costa et al., 2009 (b)). With this new, semi-automated method, it is still necessary for a cartographer to verify results, and edit results in areas which the algorithm misclassified edges or attributes.

Habitat mapping efforts for the U.S. Virgin Islands continued with benthic habitat maps being generated for the Buck Island Reef National Monument (BIRNM), north of St. Croix beginning in April 2010 and ending in January 2012 (Costa et al. 2012). Classification in this region was conducted using a combination of aerial photography, lidar, and four different multi-beam echosounders, at depths ranging from 0-1,830 meters. Classification accuracy assessment was conducted for regions of depth less than 50 meters (approximately the maximum depth measured with lidar), and the results showed overall classification accuracy ranging from 81.4% to 94.4%. Habitat delineation and classification were performed with the same semi-automated approach, with lidar reflectance used as an ancillary data source. These lidar reflectance proved valuable, assisting in identifying differing habitat types not apparent in acoustic imagery.

Benthic habitat maps generated thus far have covered much of the Virgin Island Coral Reef National Monument. Results of this research will be used to update many regions that have not been mapped since 2001, and to fill in gaps in previous habitat maps previously classified as ‘unknown.’ In total, > 119 square kilometers of underwater regions have been mapped with the EAARL-B as a part of this effort, approximately 33 square kilometers of that representing previously unmapped or ‘unknown’ classification.

1.5 Review of Related Work

The use of waveform features (shape-based metrics that can be computed from the return waveform), beyond amplitude, to provide additional information about surface characteristics and other parameters of the sensed environment, is a topic that has been explored in previous research. Collin et al. 2011 used return waveform features, along with features derived from the bathymetric surface, as predictors for epi-macrobenthic species diversity metrics in a project site in the Gulf of Saint-Lawrence, Quebec. Parrish et al. 2014 investigated the use additional waveform features to model uncertainty in coastal salt marsh environments, and found pulse width to account for over 50% vertical uncertainty between

lidar derived positions and ground control points. Rogers et al. 2015 further explored the use of lidar waveform features to predict salt marsh vegetation biophysical parameters. Parrish et al. 2016 (b) used Riegl reflectance and pulse shape deviation values from a Riegl VQ-820-G data set acquired by NOAA's National Geodetic Survey (NGS) with minimal post processing to produce seagrass habitat maps for Barnegat Bay, New Jersey. This research aims to extend these capabilities to EAARL-B waveforms and to improve the predictive capability of lidar waveform derived metrics through the use of radiometric calibration, to aid in the ability to describe complex coral reef ecosystems.

Bottom reflectivity can be derived from bottom return peak amplitude by inverting the bathymetric lidar range equation. Estimating field-of-view loss, the loss in signal strength due to photons being scattered outside the receiver field of view, can be difficult, as it is a function of optical properties of the water column, water depth, the receiver field-of-view, flying altitude, the initial diameter of the transmitted beam, and the divergence of the transmitted beam (Tuell & Carr 2013). One method of approximating the full field-of-view loss expression using a simplified proxy equation with a look-up table containing coefficients (Tuell & Carr 2013, and Carr & Tuell 2014). Feygels et al. 2003b approximated scattering coefficients and inherent optical parameters of the water using variable, or multiple, field-of-view receivers simultaneously to derive scattering coefficients. This required the use of narrow, wide, and intermediate field-of-views.

Because inverting the bathymetric lidar equation to solve for surface reflectance requires extensive knowledge of both the system and environmental conditions at the time of data collection, it is common to instead focus on the relative reflectance of the bottom return. Rather than give a direct value of the reflectance of the bottom surface, relative reflectance provides an indication of reflectance with respect to surrounding points. Narayanan et al (2009) calculates this value by taking the ratio of the bottom return for one point, to each other point within a 20 meter radius. Bottom returns are corrected using a fixed assumed attenuation coefficient. Then various statistics (minimum, maximum, average, median and standard deviation) are calculated for distribution of relative bottom reflectance values at each point.

Wang and Philpot (2007) apply two peak bottom amplitude corrections related to the angle of the incident pulse with respect to the normal vector of the seafloor. The first is a correction for retro-reflectance, in which they determine correction parameters using laboratory measurements with an assumption that all that all bottom materials are equally diffusive. The second angle of incidence

correction is for pulse stretching, which is based on the analytical simulations of Steinvall and Koppari (1996). The direct applicability of these corrections to other project sites and systems may be limited though, due to the correction coefficients being derived in a lab environment with an assumed diffusivity.

The predominant byproduct of bathymetric lidar reflectance products is a shallow water habitat map (Collin et al., 2008; Chust et al., 2010; Costa et al., 2009 (b)). Different approaches described in the published literature to date vary in terms of: 1) the waveform properties/features used in classification, 2) the level to which the waveform features are calibrated, and 3) the habitat classification scheme. Collin et al. 2008 used data collected with the Optech Scanning Hydrographic Airborne Lidar Survey (SHOALS) system to classify habitats using principal component analysis (PCA). First a set of ten waveform features were calculated from the return signal, then these features were regressed against depth and the residuals were used to perform classification. The correction and waveform generation procedures developed in Collin et al. 2008 have been used for a variety of applications. Long et al. 2010 used waveform features derived using the Collin et al. 2008 procedures to assess the correlation between bathymetric lidar waveforms and bedform morphology. Collin et al. 2012 used topographic and bathymetric waveform features to create a seamless habitat map of above water submerged regions. While these studies have shown that the full-waveform capabilities of bathymetric lidar have a broad range of applications when it comes to characterizing coastal regions, the artifact correction is limited to a non-linear regression against depth, without the incidence angle of the laser beam on the seafloor being accounted for. Data for each of the above studies were collected with the SHOALS, which has a fixed 20° forward scan angle. The forward scanning design of this system results in an incident pulse that has a nearly uniform angle from vertical across the width of the swath, thus mitigating artifacts that are more apparent in a system that scans back and forth, nearly through nadir, such as the EAARL-B.

1.6 Contributions of this Research

The motivation of this research lies not only in the immediate downstream products that it will be used to generate, but also in the methods being developed. Prohibitively-large data volumes are an inherent problem when working with waveform lidar. The procedures developed in this study were created to be passed on and used in future projects involving the EAARL-B system. The EAARL-B was not designed to be used for reflectance mapping, as will be addressed in in section 1.2. With the procedures outlined in this thesis, the functionality of the system is expanded. Adding products that the EAARL-B can be used

to create increases the versatility of the system, allowing for a wider variety of research projects to be conducted in the future.

The specific goals of this research are as follows:

- Design, implement and test correction procedures for the EAARL-B bottom return peak amplitude values.
- Generate relative reflectance mosaics for the area to the south of St. Thomas and St. John, U.S. Virgin Islands.
- Generate waveform feature surfaces from additional waveform features (area under the curve, skewness, standard deviation), as well as procedures for producing waveform feature products that can be passed on to other researchers.

The methodology outlined in this thesis serves as the culmination of years of research and experimentation to reach the optimal intensity correction workflow outlined in subsequent chapters. The importance of past efforts to perfect not only the correction applied to raw peak bottom return amplitude values, but also to generate tools and procedures to generate relative reflectance mosaics cannot be understated.

Initial processing methods, evaluated using data from Superstorm Sandy mapping efforts (Kinney et al. 2016), resulted in development of initial angle of incidence correction methods, correction of waveform feature exporting issues within ALPS, and development of histogram normalization and batch gridding tools (Parrish and Wilson (2015)). Early work with U.S. Virgin Islands data, limited to the shallow water region surrounding Buck Island, north of St. Croix, necessitated the development of a depth correction, as this location contained a much more highly variable depth range (~0-30m) compared to that of the Superstorm Sandy project (~0-4m) (Parrish, Forfinski and Wilson, 2016). Work on the St. Croix project site also led to improved gridding procedures.

2. METHODS

2.1 Workflow

The final workflow for generating relative reflectance mosaics, developed as a part of this research, is depicted in green in Figure 2-1. Correction, histogram normalization, and gridding procedures are described in subsequent sections. It should be noted that this workflow is intended for very large datasets, in which the semi-automated histogram normalization in Swath Normalize may require data to first be gridded at a coarse resolution (10-20 m GSD), in order for the program to be able to render contrast and brightness adjustments without crashing, or taking a long time to apply user specified adjustments. The object based image classification, in which the mosaics generated by this research are an input, is a topic of future work and is not assessed in this research.

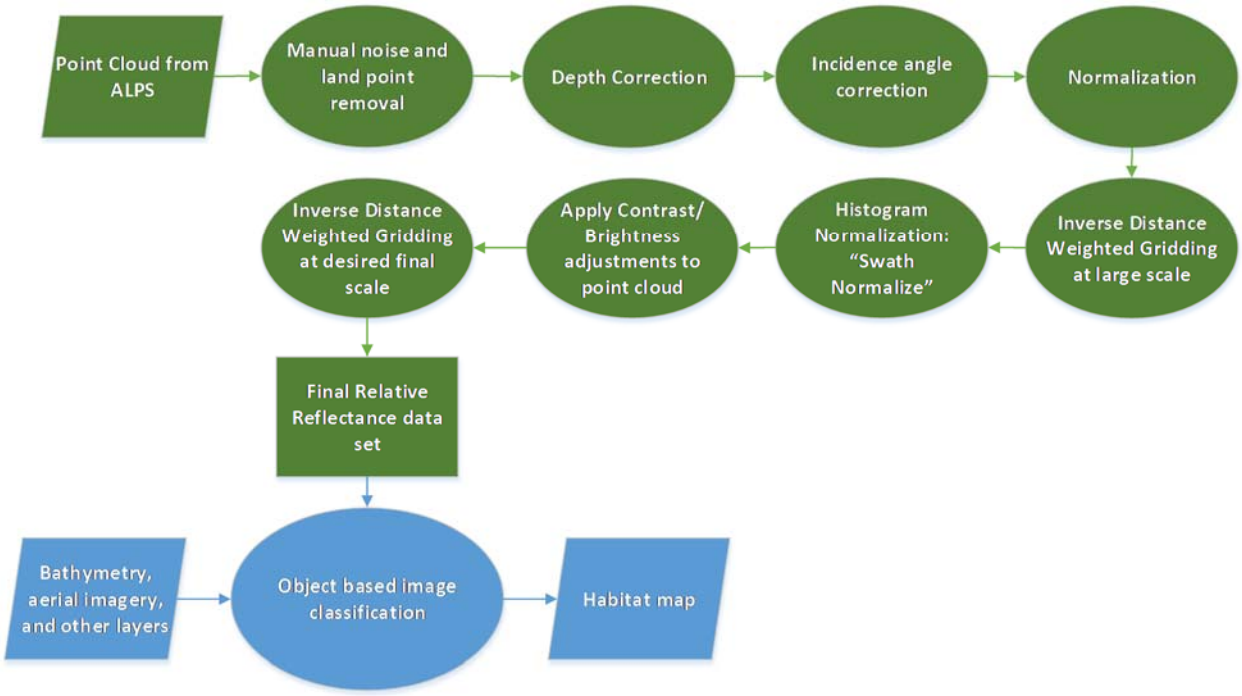

Figure 2-1: Workflow diagram for generating relative reflectance mosaics.

2.2 Corrections

Calibrating waveform peak amplitude returns to give true bottom reflectance requires extensive knowledge of both the system used to collect the data, and the environment in which the data are collected. The full bathymetric lidar range equation (Eq. (2)) (Kashani et al., 2015) contains terms that are not readily available in most circumstances. There are multiple versions of this equation, each with

different levels of simplification and assumptions (Collin et al.; 2008, Narayanan et al.; 2009, Tuell & Carr, 2013; Tuell et al., 2015, Wang & Philpot, 2002), and each generally similar to the following:

$$P_R = \frac{(m)P_T\eta\rho F_p A_r cos^2(\theta)}{\pi(n_w H+D)^2} exp(-2\mathrm{n(s},\omega_0,\theta)KDsec(\phi)) \quad (2)$$

where, P_r = received power, P_T = transmitted power, η = system optical efficiency factor, ρ = reflectance of bottom, F_p = loss due to insufficient FOV, A_r = effective area of receiver optics, ϑ = off nadir transmit angle, n_w = index of refraction of water, H = altitude of lidar above water, D = bottom depth, $n(s, \omega_0, \vartheta)$ = pulse stretching factor, s = scattering coefficient, ω_0 = single scattering albedo, K = diffuse attenuation coefficient of water, and ϕ = nadir angle of lidar after entering the water. Solving equation 2 for bottom reflectance would yield true bottom reflectance. However, factors relating to the lidar system (P_T, η, F_P) are not always given by the manufacturer, and factors relating to the environment ($n(s, \omega_{00}, \theta)$, s, ω_0, θ, K) can be difficult to measure and may not be consistent across projects covering large areas with data collected over multiple days.

In this work, a data-driven approach is taken to correct artifacts in the data: the data itself is used to drive correction coefficient determination. A two-step correction procedure is used (Parrish and Wilson, 2015). The first step is to apply intensity corrections, corresponding to Level 1 processing, as defined in Kashani et al. (2015). Specifically, corrections are applied for: 1) depth, and 2) angle of incidence.

2.2.1 Depth Correction

A simplified version of the lidar range equation adapted from Guenther (1985) is:

$$P_R = P_T W\rho exp(-2KDsec(\phi)) \quad (3)$$

This equation is adapted from the full lidar range equation, with simplifying assumptions being made. Using this equation requires the assumption that systematic losses from the lidar system, the nadir angle of the beam after entering the water, and that the altitude of flying height above the water is relatively large compared to depth. Taking the natural log of Eq. (3) as shown in Wang and Philpot (2007), yields:

$$ln(P_R) = ln(P_T W) + ln(\rho) - 2KDsec(\phi) \quad (4)$$

With the assumption that the transmit power and system losses are constant throughout the survey, the natural log of the bottom reflectance is linearly related to the natural log of the received power at a rate that is a function of the diffuse attenuation coefficient of the water, *K*, and the slope length of the lidar pulse in the water ($D\sec(\phi)$).

Determining the rate at which the natural log of the received power is deteriorating through the water column is done through calculating the linear regression of natural log of the bottom return against slope length. Figure 2-2 shows a heatmap created using points from entire day of data collection with the resulting linear best fit line. These heatmaps have been used throughout this research as a tool to visualize trends in large amounts of data. The color scale can be interpreted as the 'hotter' regions being those of high point concentration, with dark regions containing relatively low concentration of points. Exact color scale values are dependent on the amount of points used to generate each heatmap.

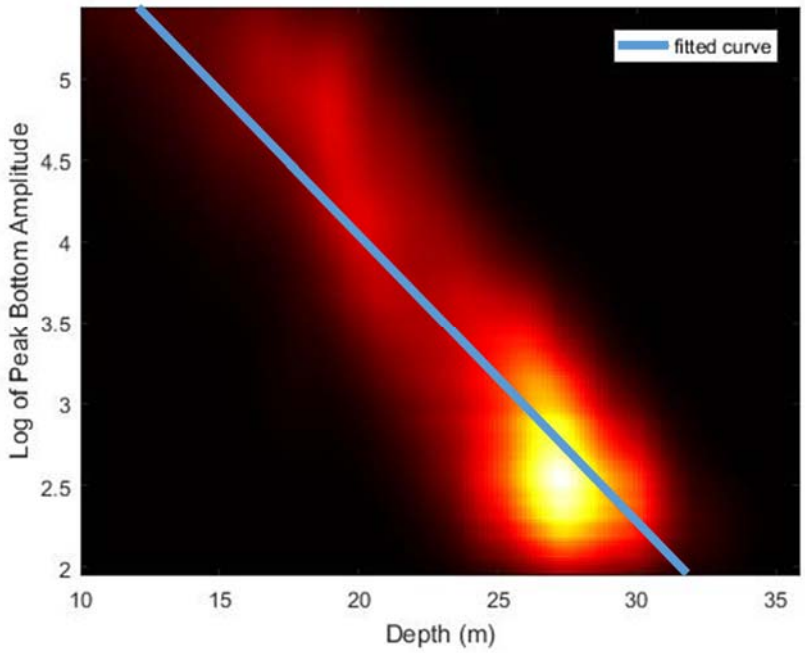

Figure 2-2: Heatmap of the natural log of the peak bottom return amplitude against depth.

Using the slope and intercept of the linear best fit shown above, the correction equation is given as follows:

$$I' = ln(I)/(a \cdot D \cdot sec(\phi) + b) \quad (5)$$

2.2.2 Angle of Incidence Correction

One of the simplifying assumptions to using Eq. (3) is that the system collects data with a scan geometry containing a nearly constant nadir angle. With many systems, the geometry is such that on the pulse is emitted in a forward tilted direction, and the angle from vertical on the water surface is consistent across the width of the swath. The EAARL-B has a very small forward scan angle, resulting in a highly variable nadir angle. This creates a pronounced reduction in received power as the scan angle increases towards the outer edges of the swath.

Similarly to the way in which the depth correction parameters are determined and applied, corrections for angle of incidence are determined through a data-driven approach. The trend of intensity values that have been corrected against depth are regressed against angle of incidence to determine correction parameters. The incidence angle correction is computed as follows:

$$I'' = I'/(a' * cos^{b'}(\theta)) \quad (6)$$

where a' and b' are parameters determined as described above, that describe the "shininess" (specular or non-Lambertian nature) of the material. This correction represents a simplified version of the Phong reflectance model (Jutzi & Gross, 2009 and Phong 1975). The Phong reflectance model is an empirical method, originally designed for computer graphics, of representing how much light is reflected from a source to a receiver, dependent on the angle between the incident light, the reflectance vector to the receiver, and the surface normal. With an assumed vertical surface normal, and with the incident pulse and receiver field of view located coaxially, the angle of interest becomes the nadir angle, also described as the angle of incidence. Figure 2-3 shows a heatmap of peak bottom amplitude values corrected for depth against the angle of incidence.

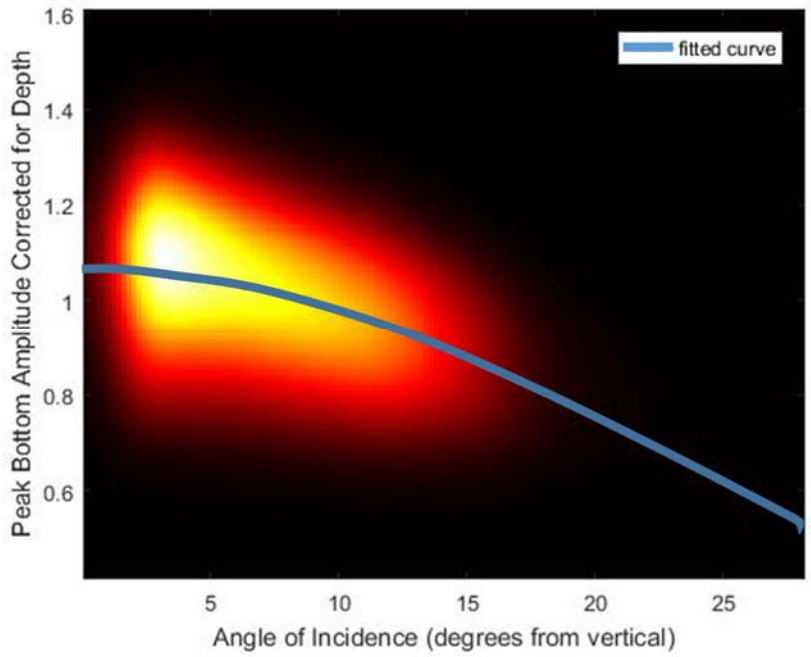

Figure 2-3: Heatmap of the peak bottom amplitude corrected for depth against angle of incidence.

2.2.3 Iteration

An underlying assumption in the correction procedures described above is that the points used to derive the correction parameters have the same "true" reflectance; hence, it is important that the subsets of points used as input are collected from a homogeneous bottom type. One of the advantages of using bathymetric lidar over conventional passive remote sensing mapping techniques is the extended depth range. This becomes a disadvantage for delineating regions of uniform bottom type in project sites that have only been characterized by aerial or satellite photography, have out-of-date habitat maps, or have not been mapped previously.

For the EAARL-B deep receiver channel, an initial approximation of correction parameters can be made using all of the points calculated for given day. Then the resulting point cloud can be used to assist in delineation of uniform bottom type, typically sand. The points of uniform bottom type can then be used to determine final correction parameters.

2.3 Histogram Normalization

The next step in our procedure is to apply a histogram normalization, corresponding to Level 2 processing, as defined in Kashani et al. (2015). This is achieved by first matching points of overlapping point clouds that are within 1 meter of each other, with the assumption that points within 1 meter of each other should be representative of the same bottom type. The distribution of each set of match points is analyzed, then the standard deviation and mean of each is used to perform the initial normalization. Because this normalization procedure only uses points that are near each other, it is important to combine regions with sufficient overlap.

A second histogram normalization step is taken to ensure seamless final mosaics are created. This is achieved using custom software called *Swath Normalize*, depicted in Figure 2-4, which was developed as part of this research. Swath Normalize applies semi-automated histogram scaling and shifting to adjust the contrast and brightness across adjacent rasters. Overlapping gridded data are adjusted by the user until overlapping regions visually match. Contrast and brightness adjustments are then applied to the point clouds, combined with each other, and the final grids are created.

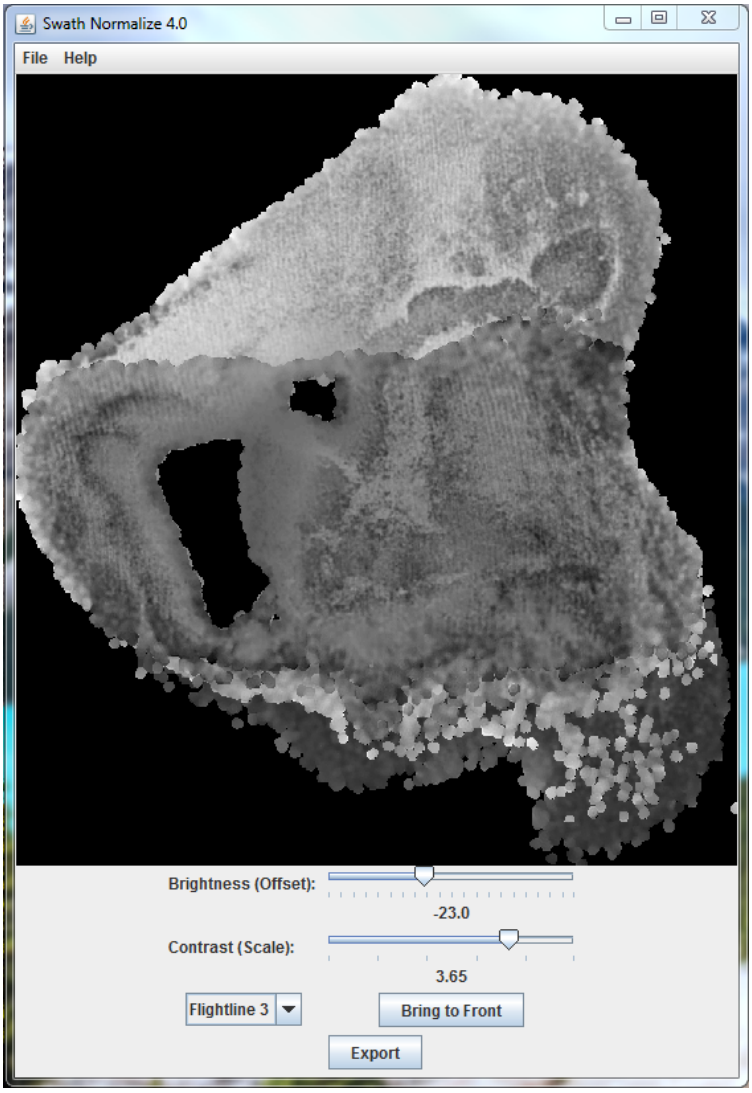

Figure 2-4: *Swath Normalize*, semi-automated histogram normalization program.

2.4 Gridding

An inverse distance weighted method was chosen for gridding the relative reflectance products created in this research. Using inverse distance weighting is advantageous in gridding these types of products for a number of reasons. Seamline artifacts between overlapping flightlines are reduced, creating a more uniform representation of regions in which the angle of incidence correction has been either over- or under-applied. Combining multiple days' worth of data and gridding them together results in a blended final mosaic, and reduces the effect of outliers that may be present in one dataset, but not another.

The effect of combining flightlines before gridding can be seen in Figure 2-5. Visual inspection shows that seamline artifacts across flightlines are effectively reduced, allowing actual bottom type variation to be more effectively represented. Coordinates depicted in Figure 2-5 and all subsequent map figures are referenced to NAD 83 and projected in UTM Zone 20 N.

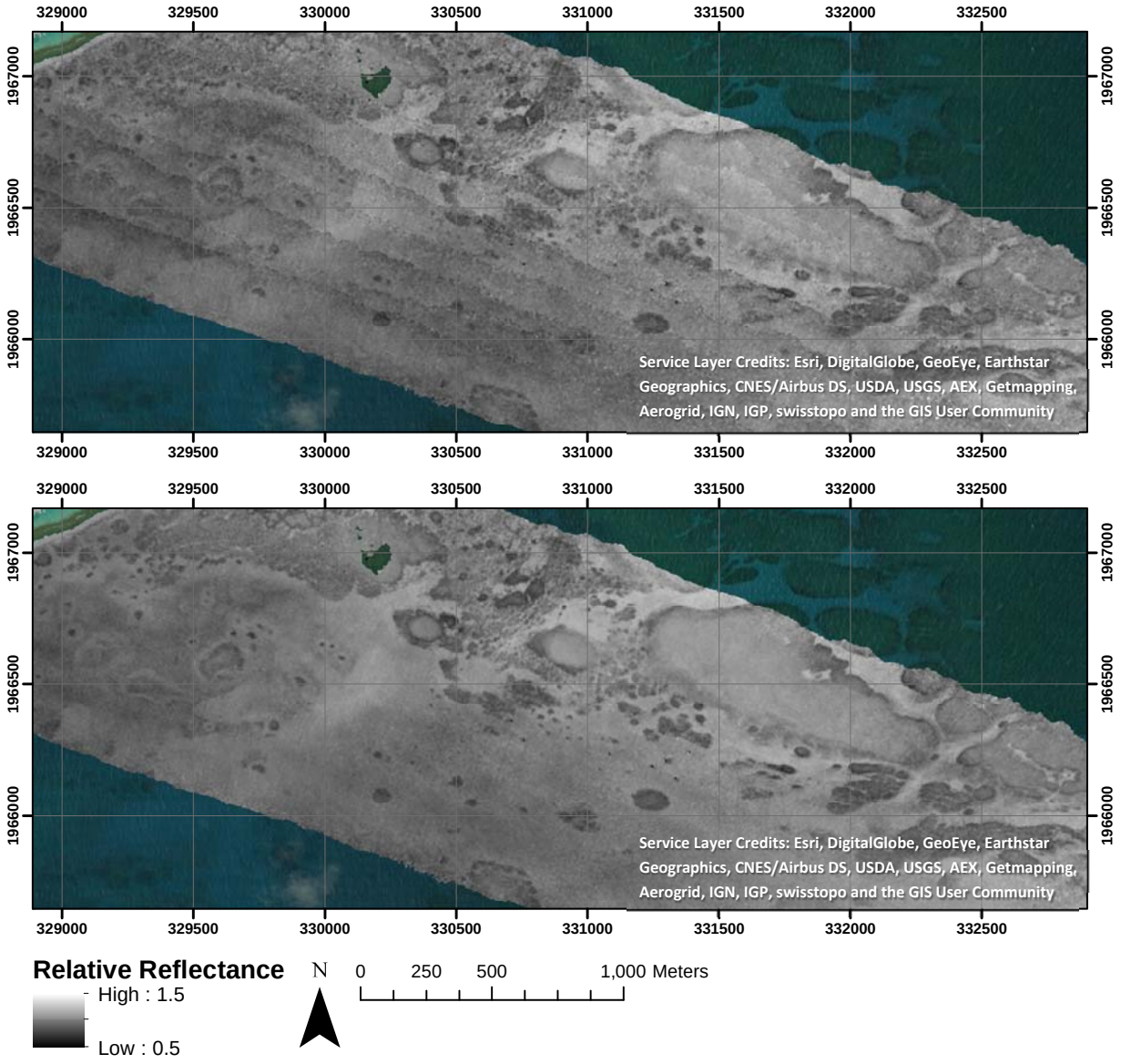

Figure 2-5: Gridded relative reflectance of St. Croix. Top: Flightlines gridded individually. Bottom: Flightlines combined before gridding.

3. EXPERIMENT

3.1 Study Site

The area of interest of this research is located to the south of St. Thomas and St. John in the U.S. Virgin Islands. This area is of high interest to the local population, especially including those who rely on the coral reef ecosystems in the region for tourism, fishing, and recreation.

In March of 2014, the U.S. Geological Survey (USGS) in cooperation with the National Oceanic and Atmospheric Administration (NOAA) Coral Reef Conservation Program collected bathymetric lidar data for the regions with the second-generation Experimental Advanced Airborne Research Lidar (EAARL-B). Processing of digital elevation models of the region has already been conducted (Fredericks et al. 2015) by USGS, but relative reflectance products are needed to assist with benthic habitat classification procedures.

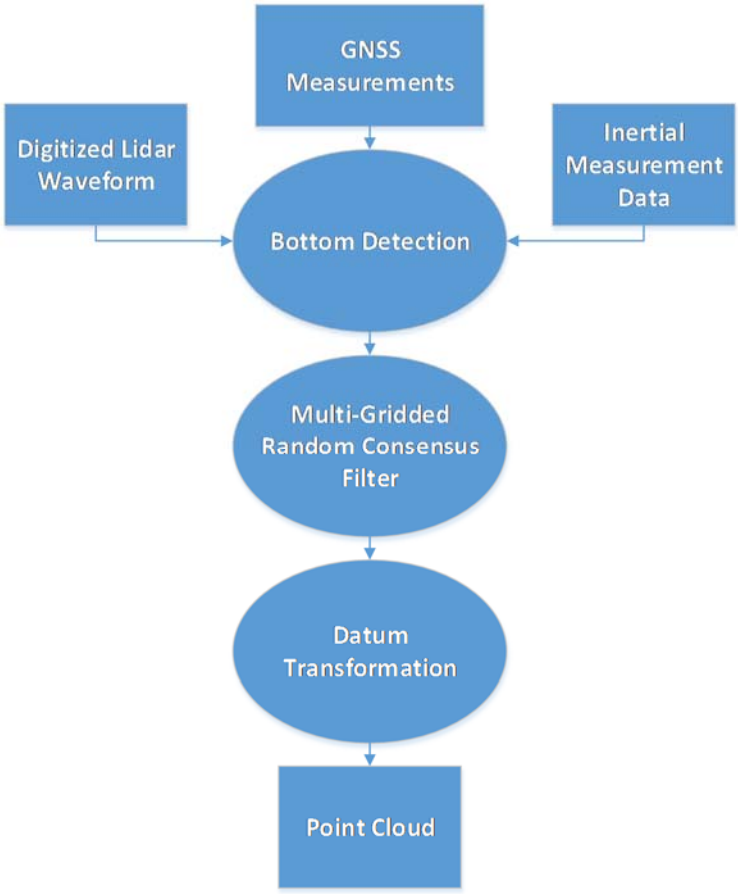

Figure 3-1: ALPS Lidar waveform processing procedure.

The processing procedure used to generate the point cloud data that form the input to our workflow is depicted graphically in Figure 3-1. First, the digitized lidar waveforms are combined with GPS and inertial measurement data to generate point positions and calculate waveform features. The resulting point cloud can contain a significant amount of noise. These noise points are created from the bottom detection algorithm misinterpreting a part of the waveform as a surface. The ALPS program also includes a random consensus filter, modeled after the random sample consensus (RANSAC) paradigm (Fischler & Bolles, 1981) to remove noise. The filter works by first partitioning the data into grid cells. The distribution of elevation values within each grid cell is used to form a consensus of what the elevation of the grid cell should be, then all points outside a set elevation range are removed. The function also has the capability to shift the grid cell boundary when forming a consensus. This shift allows for points at the edge of the cell boundaries to be less likely misclassified as noise. Position values are then referenced to NAD 83 and projected in Universal Transverse Mercator (UTM) (Zone 20 N in the USVI). Lastly, position and waveform feature information are exported to an ASCII file, which is then used as the input for this research.

The methods described in the previous chapter were tested in two different areas of interest (AOIs): a smaller AOI for the waveform feature mapping and a larger AOI for relative reflectance mapping. The small AOI comprised a 1.5 km^2 region roughly centered on Flat Cays, south of St. Thomas. This area was selected for its high diversity in known habitat types, its large depth range (0-28 m) over a relatively small spatial extent, and because the region was covered on multiple flight dates, resulting in a high point density ranging from 1-4 points per square meter (Costa et al. 2016). This project site will serve to analyze the usefulness of corrected waveform products in fine scale habitat complexity characterization. *In situ* data has since been collected for the region, and will be used in later project phases for enhanced ecological mapping and analysis. Meanwhile, the larger AOI (which fully encompasses the smaller AOI) consists of the entire ~550 km^2 area mapped by USGS with the EAARL-B south of St. Thomas and St. John in March 2014. The analysis for this larger AOI focused solely on relative reflectance mapping, rather than generation and analysis of the full suite of bottom return waveform features.

3.2 Data Collection

The airborne lidar data were collected using the EAARL-B system described previously. The data acquisition parameters (Fredericks et al. 2015; Wright et al., 2016) are summarized in Table 3-1. Data were collected for the St. Thomas and St. John project site on March 7th, 8th, 11th, 12th, 13th, 14th,

17th, 18th and 24th of 2014. Extents of data collected can be seen in Figure 3-2. Data were collected with both the EAARL-B deep (large FOV) and three shallow (small FOV) receiver channels, enabling seamless mapping in depths of up to approximately 35 meters.

Table 3-1: Data acquisition parameters.

Acquisition parameter	**Setting/value**
Flight altitude	300 m
Flying speed	55 m/s (110 kts)
Scan angle	5° forward, 22° across-track
Measurement rate	15-30 kilohertz
Aircraft	Cessna 310
Swath width	240 m
Point spacing	0.5-1.6 meters
Laser footprint	30 cm
Pulse width	900 ps
Laser wavelength	532 nm

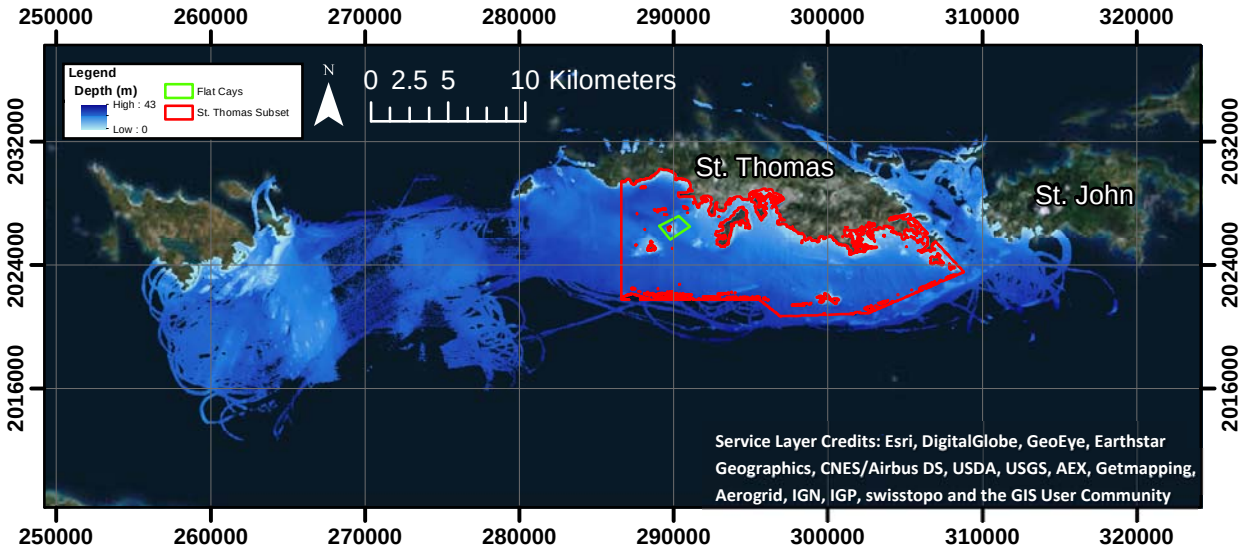

Figure 3-2: Project location and extents for data processed as a part of this experiment.

3.3 Flat Cays Full Waveform Features

Project extents for the Flat Cays region of interest can be seen in Figure 3-3. Viewing the ESRI World Imagery available for the area illustrates the need for reflectance products for deep regions. Shallow regions near the island could likely be classified solely from imagery, as the seafloor is visible in the imagery. However, in the deeper portions of the site, the bottom cannot be seen in passive, optical imagery, while the bottom was detected in the EAARL-B data.

This submerged area represents approximately 1.5 km^2, and was covered on three separate collection dates. After noise removal, a total of 1.4 million points were used to generate corrected waveform products.

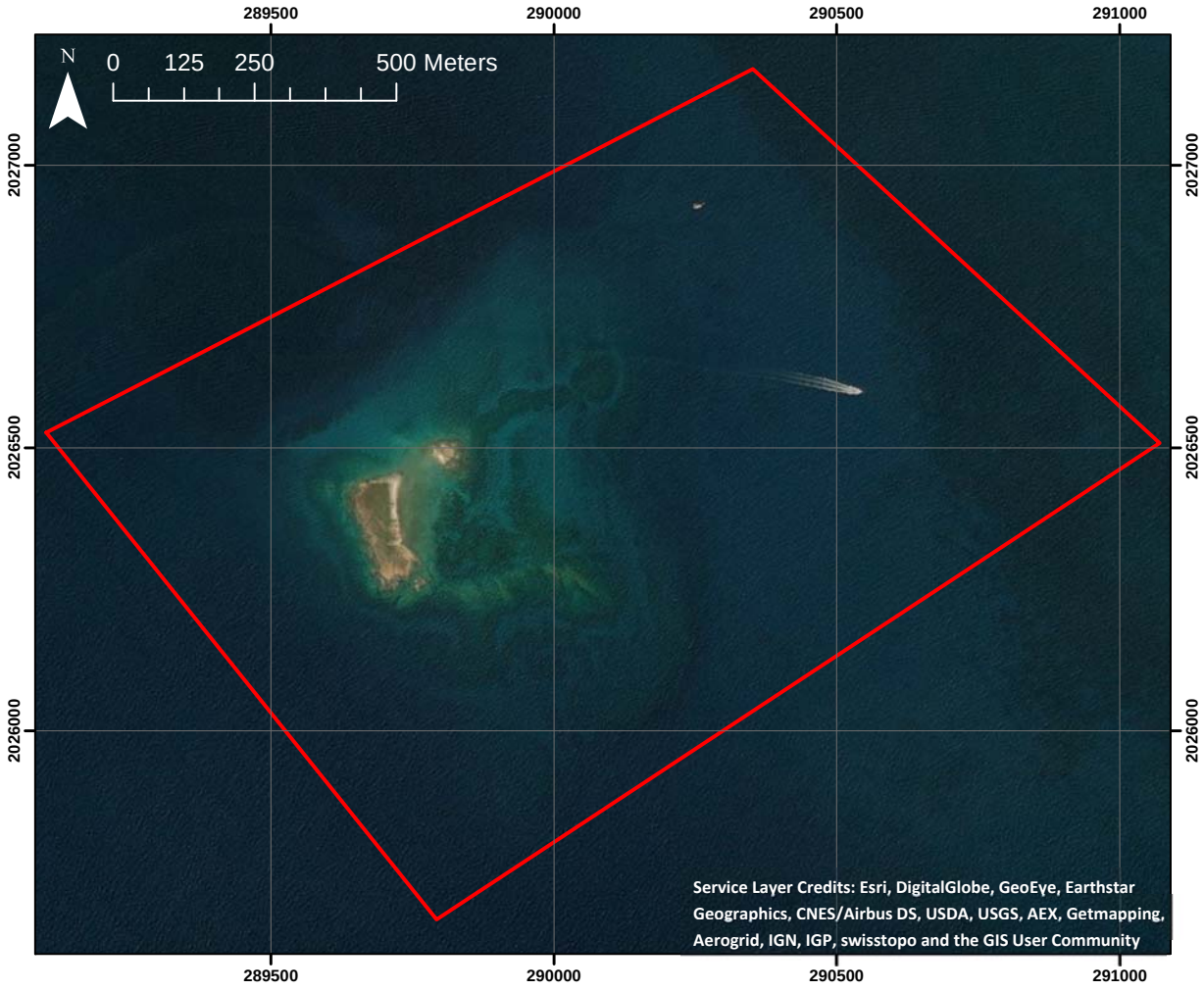

Figure 3-3: Flat Cays area of interest project extents with ESRI basemap.

Methods described in this research were primarily designed and tested for correcting for artifacts affecting peak bottom return amplitude values. Investigation into other features derived from the bottom return waveform shape revealed similar trends for each feature relative to depth and angle of incidence. Therefore, as a first pass, the methodology described in Chapter 2 was applied to create corrected waveform feature products, and for normalizing results across different collection dates and for combining data across deep and shallow receiver channels. Future work may involve dedicated corrections for each individual waveform feature (see Conclusions). Gridded waveform feature products for the Flat Cays region of interest can be seen in Figure 3-4.

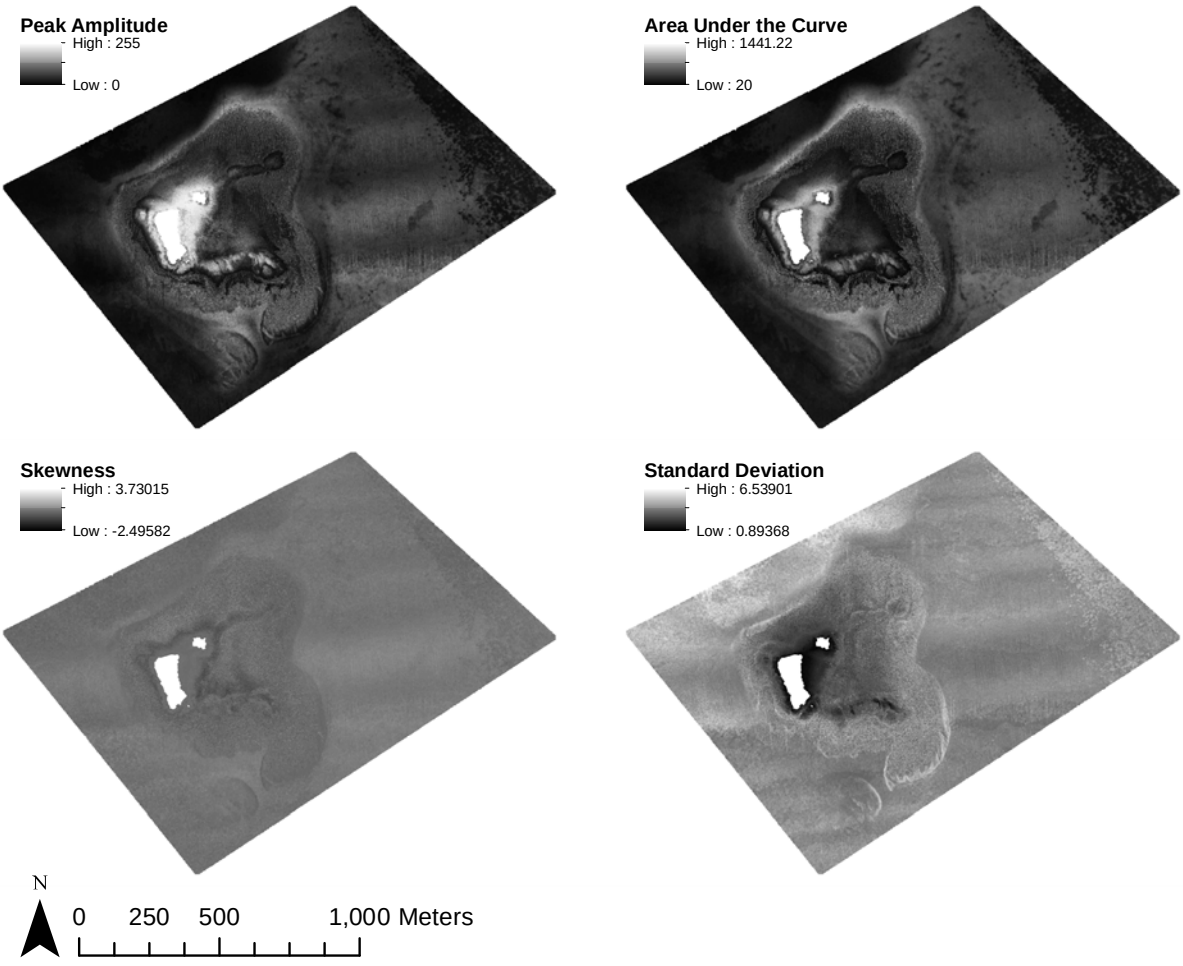

Figure 3-4: Gridded uncorrected waveform features for Flat Cays.

3.4 St. Thomas Relative Reflectance Mosaic

Representing approximately 119 km^2 of submerged area, habitat maps to be generated using relative reflectance products represent an extensive update to the current habitat maps of the region. After automated and manual removal steps, approximately 84.4 million points were used to generate final relative reflectance mosaics with a 3 meter cell size.

Because correction parameters are derived from the data, emphasis was placed on ensuring that outliers were removed from the data prior to processing. This was done by iterating the random consensus filter parameters until noise was sufficiently removed for both the deep and shallow receivers, and by manually removing all other outliers and land points that made it through the filter. Parameters used in the random consensus filter area as follows, as defined in Nagle & Wright (2016): buffer = 600 cm, width = 60 cm, n = 3, factor = 4.

Histogram normalization across different collection dates was accomplished by assessing the amount of overlap there was across each coverage. This process increased the number of match points between different data sets to ensure a large sample size of match points.

4. RESULTS

The outputs of the methods described above include seafloor relative mosaics and gridded waveform feature data sets. While these data products are, from the perspective of this project, "outputs," it is important to note that they constitute "inputs" to the benthic habitat mapping and ecological assessments to be conducted by NOAA NCCOS. The final assessment of the results of this work will be in the form of classification accuracy assessments performed on the habitat maps and analysis of other downstream products. For assessing the data products generated in this research (i.e., seafloor relative reflectance mosaics and gridded waveform features), reference data (or "ground truth") are limited. Therefore, our assessments focus on: 1) visual assessment (e.g., confirming visually that our data products look consistent and are free of salient artifacts, such as seamlines, data voids and aberrant discontinuities), 2) internal consistency (e.g., agreement of relative reflectance or waveform features across deep/shallow regions within a single collection date, and across multiple dates), and 3) metrics for the correction performance (depth and angle of incidence). Particular emphasis is placed on criteria deemed to be of high importance in the generation of downstream products. While control reflectance measurements are not available for the St. Thomas area of interest, seafloor reference spectra were collected in July, 2012 around the Buck Island Reef National Monument. EAARL-B data collected as a part of this effort includes coverage of the area surrounding Buck Island, and were used to quantitatively assess methods developed as a part of this research.

4.1 Flat Cays Full Waveform

Results for the Flat Cays region of interest can be seen in Figure 4-1. The high density of points in this region, due to it being covered with multiple flightline passes, allowed for a small grid cell size to be used (0.5 m). Preliminary assessment of the results indicates a significant improvement the ability to detect seafloor bottom type variation over the uncorrected waveform feature values. These results also show a limitation to using a simplified, data driven correction method, in that unaccounted for environmental factors can impact the quality of the corrections.

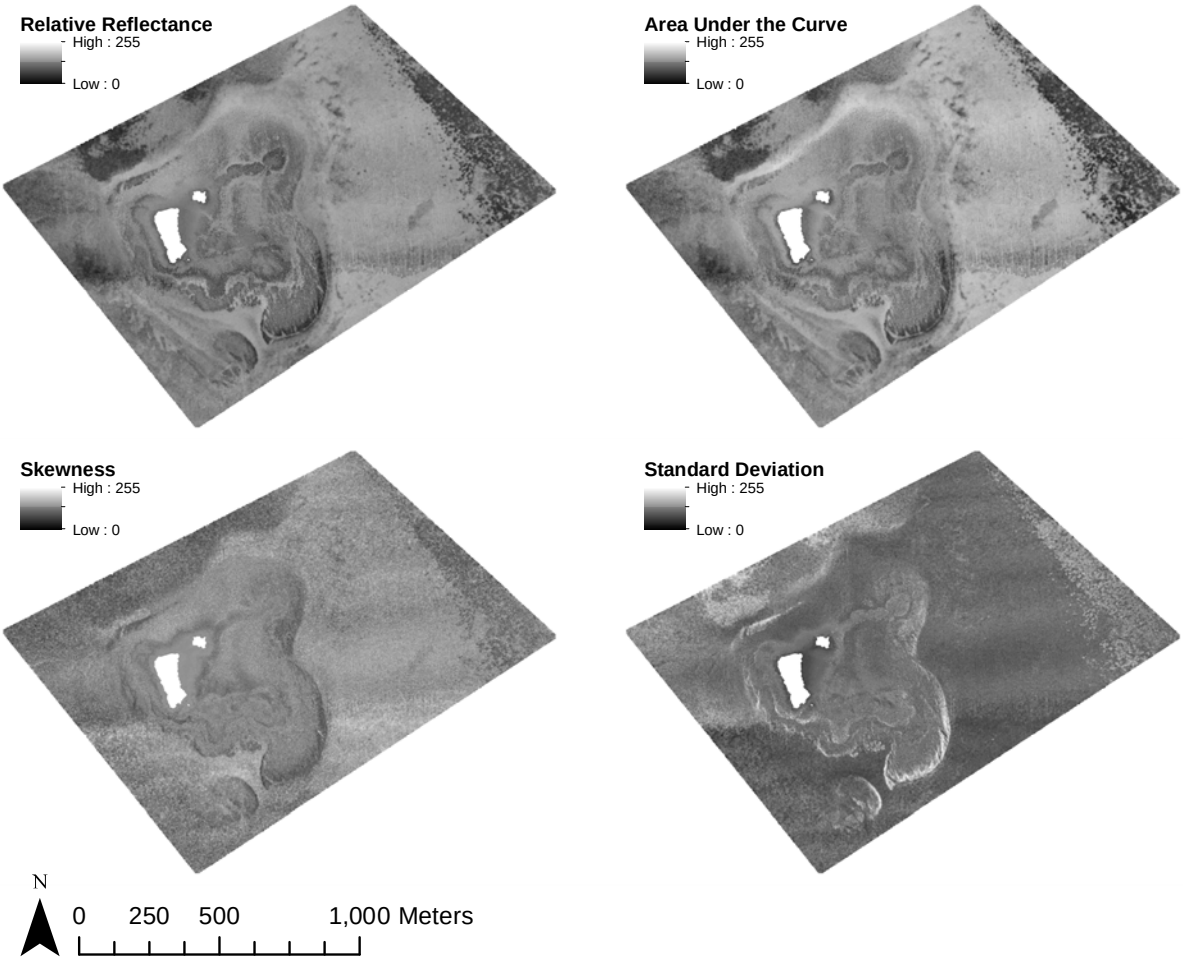

Figure 4-1: Flat Cays corrected waveform feature grids. All final grid values have been scaled to 0-255.

Coverage of this region over multiple days, and under varying conditions, allows the effect of certain environmental conditions to be examined. Bottom return peak amplitude values for one collection date exhibited across flightline artifacts not consistent with the other two collection dates over approximately the same region, even with parallel flight paths. Examination aerial photographs taken at the time of collection revealed a significant amount of sun glint, consistent with artifacts found in the waveform feature products generated from the deep-water receiver.

Because this sun glint artifact is dependent on collection geometry in relation to the elevation angle of the sun and solar azimuth at time of collection, the fitted curve used to correct for angle of incidence artifacts has a less pronounced trend to model. This resulted in some across flightline artifacts persisting in the final results.

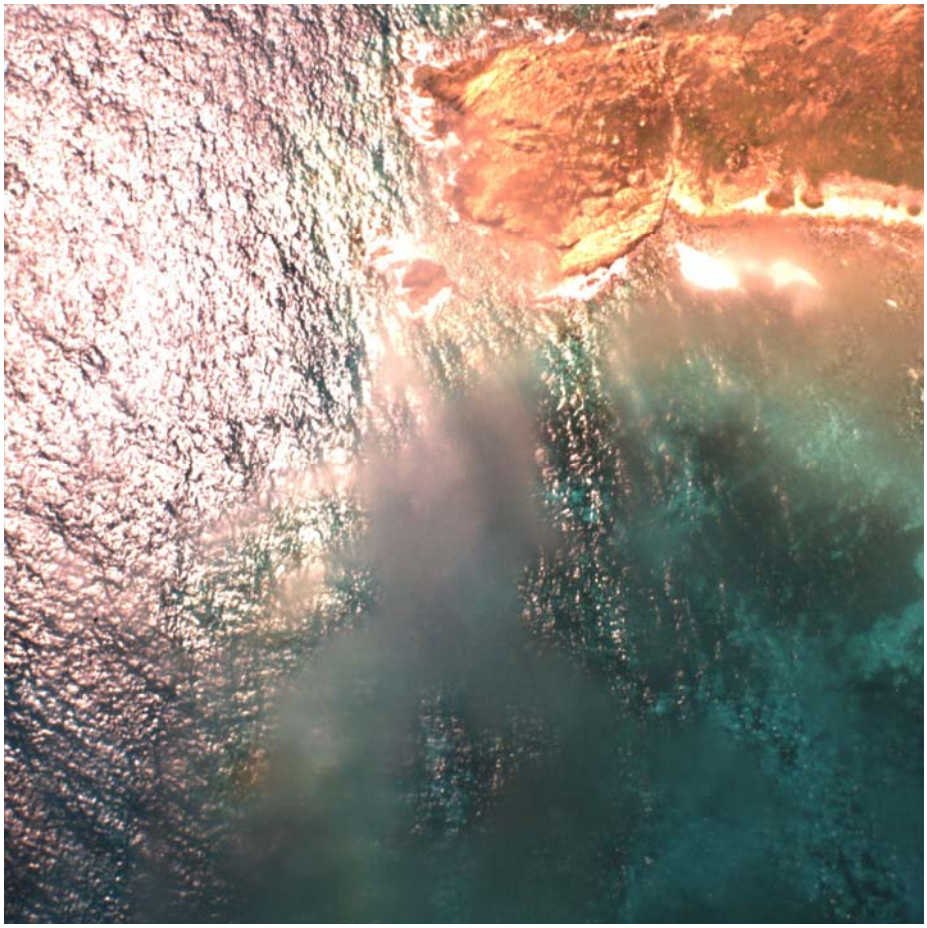

Figure 4-2: Aerial photography showing sun glint at time lidar collection.

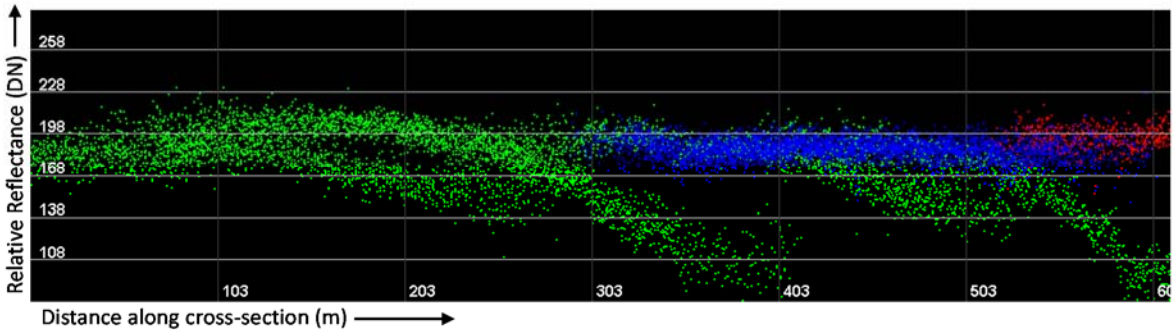

Figure 4-3: Cross section showing artifacts present in relative reflectance products collected at a time when sun glint is present (green), but not in overlapping data sets collected with the sun at a lower elevation angle.

4.2 St. Thomas Relative Reflectance Mosaic

A final relative reflectance mosaic was generated for the St. Thomas and St. John region, using a total of 84.4 million points and covering 119 square kilometers. The final mosaic represents a subset of the complete region in which data were collected as a part of this effort. This region was selected because it was deemed that this region has the corrections working the best. The assumption that a single correction parameter can be used to correct for depth and angle of incidence for an entire day presents issues with projects that have very large extents

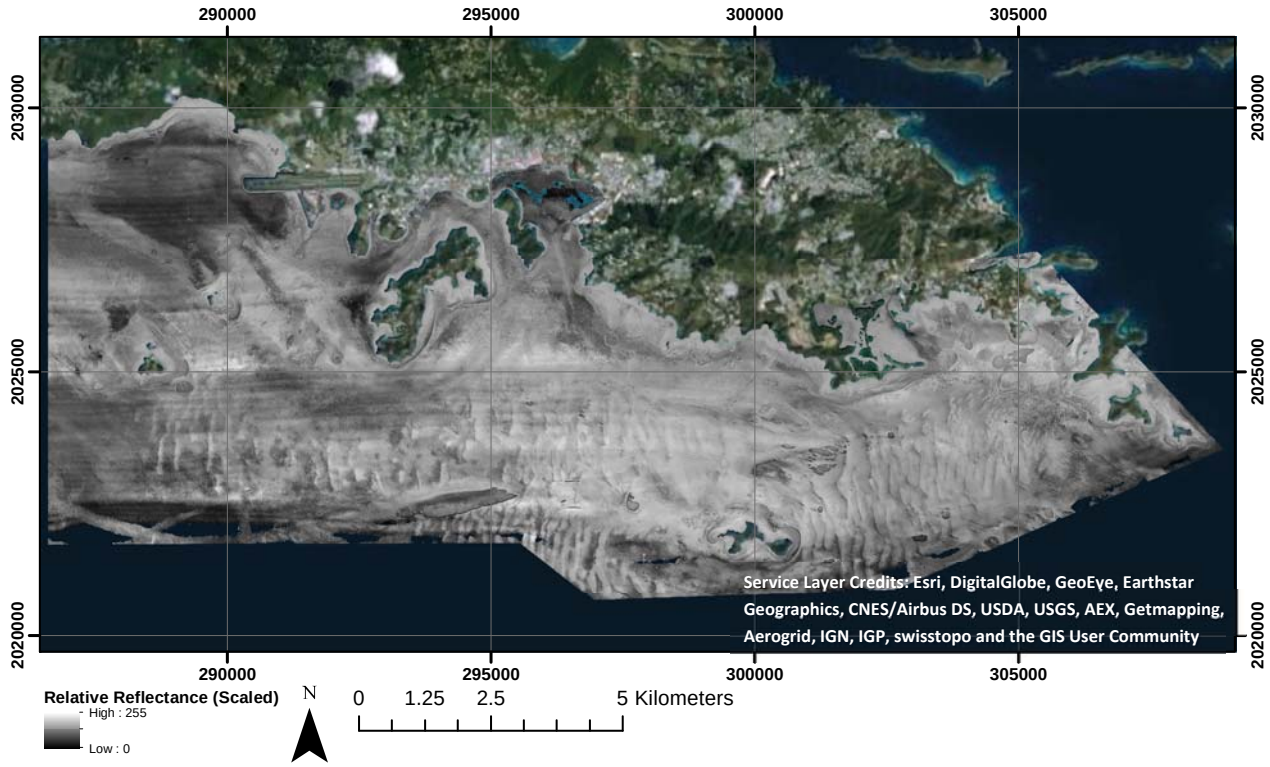

Figure 4-4: St. Thomas relative reflectance mosaic.

4.3 Quality Assessment

One of the benefits to using bathymetric lidar over aerial photography is that greater depths can be measured, which makes validation of deep-water seafloor reflectance products difficult. Assessment of position values can be done using acoustic data, but acoustic backscatter cannot be directly related to lidar reflectance. The primary method of quality assessment of results for both the Flat Cays full waveform products, and the St. Thomas and St. John mosaic was through visual inspection. This was

done through a four step process to assess the results of each correction that was applied, the histogram normalization, and through comparison to uncorrected waveform products.

4.3.1 Evaluation of Depth Correction

Evaluation of the depth correction performance was primarily done using heatmap plots showing the natural log of bottom return peak amplitude values against depth. If a uniform bottom type is used for the depth correction, this plot should show a linear trend. Non-linear trends found in this plot give indication that either multiple bottom types were used in this step, or environmental conditions have changed throughout the survey. This could be caused by localized water clarity differences or changing sea-surface conditions.

4.3.2 Evaluation of Angle of Incidence Correction

Remaining artifacts associated with angle of incidence are typically easy to differentiate from natural seafloor reflectance changes as they present parallel seam lines in the direction of flight path. Reduction or elimination of these seam lines indicates that the angle of incidence correction is working well. Cross sections across multiple flightlines were also used to check the quality of this correction. Plotting relative reflectance on the vertical of cross sections shows how well the reflectance values of overlapping flightlines intersect.

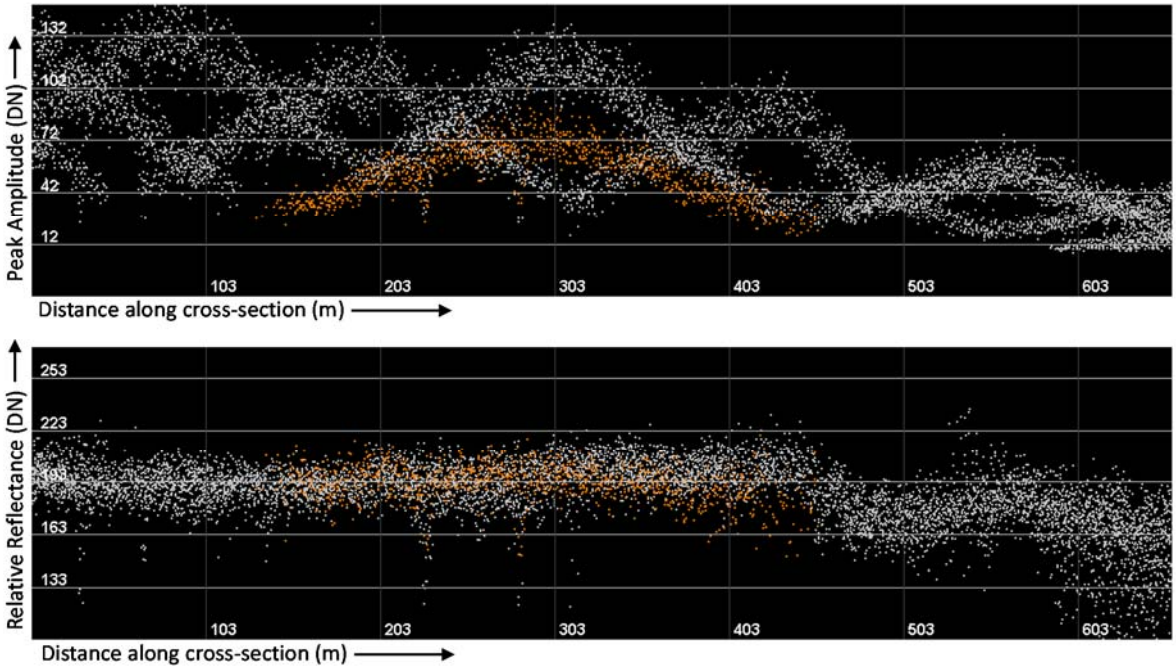

Figure 4-5: Example cross section taken perpendicular to flight paths, colored by collection date. The top cross section shows peak bottom return amplitude, the bottom cross section shows the same points after depth and angle of incidence corrections, and histogram normalization. It can be seen that the corrections had the desired effects of flattening the curves and greatly improving the consistency between the data collected on different dates.

4.3.3 Evaluation of Histogram Normalization

Histogram normalization results were evaluated using cross sections of overlapping regions. Vertical offsets, or differences in the spread of reflectance values indicate poor normalization results. Localized artifacts present in one dataset, but not another, can cause the automated histogram normalization procedure to adjust values in an unanticipated way. Adjusting contrast and brightness in Swath Normalize provides a way to visually correct and make fine-tune adjustments to adjacent datasets.

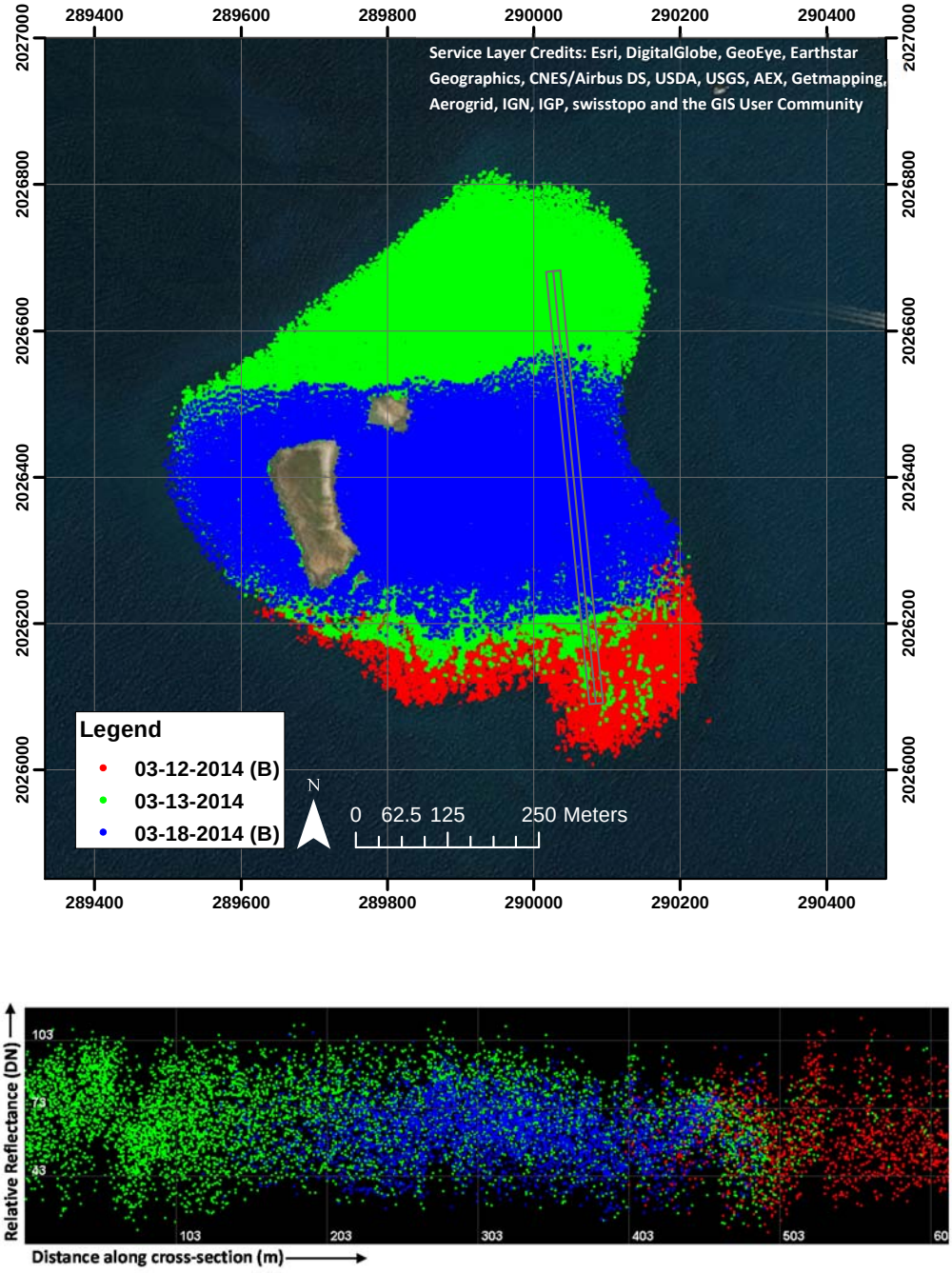

Figure 4-6: Example cross-section location (top) and cross section (bottom) used to evaluate normalization between reflectance products generated from shallow depth channels across multiple collections dates.

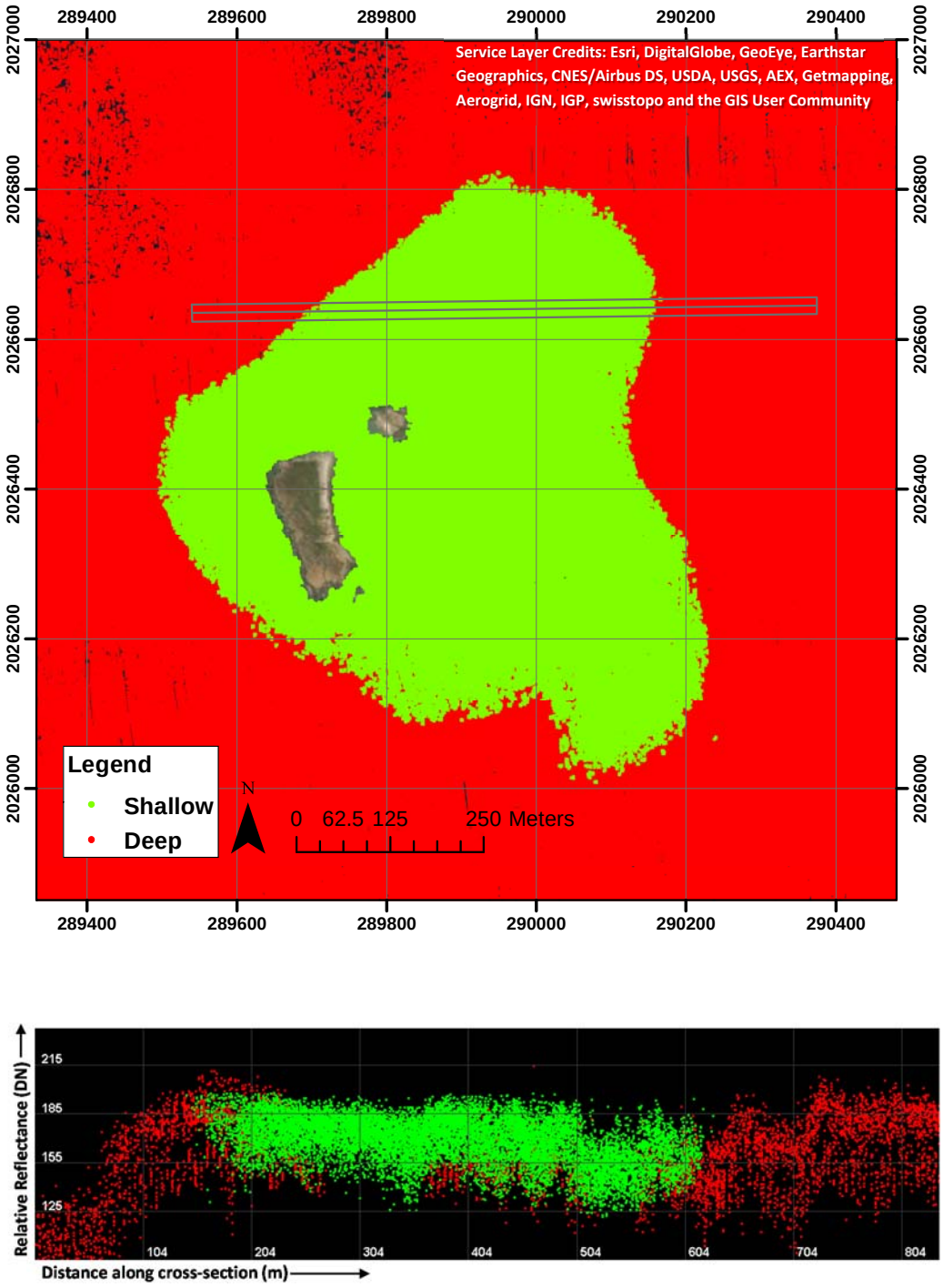

Figure 4-7: Example cross-section location (top) and cross section (bottom) used to evaluate normalization between reflectance products generated from deep and shallow depth receiver channels.

4.3.4 Comparison of Corrected to Uncorrected Results

Qualitative visual assessment was conducted as a final step in evaluating results. Comparison of relative reflectance, or other corrected waveform feature values, to uncorrected values can show features that are identifiable in final products that were not visible or hard to detect in the uncorrected products. Though some artifacts may remain in the final products, as identified in the quality assessment procedures above, an improvement in feature detection capability is seen as an improved product.

Figure 4-8 shows relative reflectance products generated from the EAARL-B deep water channel for a single flight date. In this region, seamline artifacts have been reduced, or eliminated, in most areas. Depth artifacts have been reduced, such that changes in bottom type can likely be distinguished and delineated.

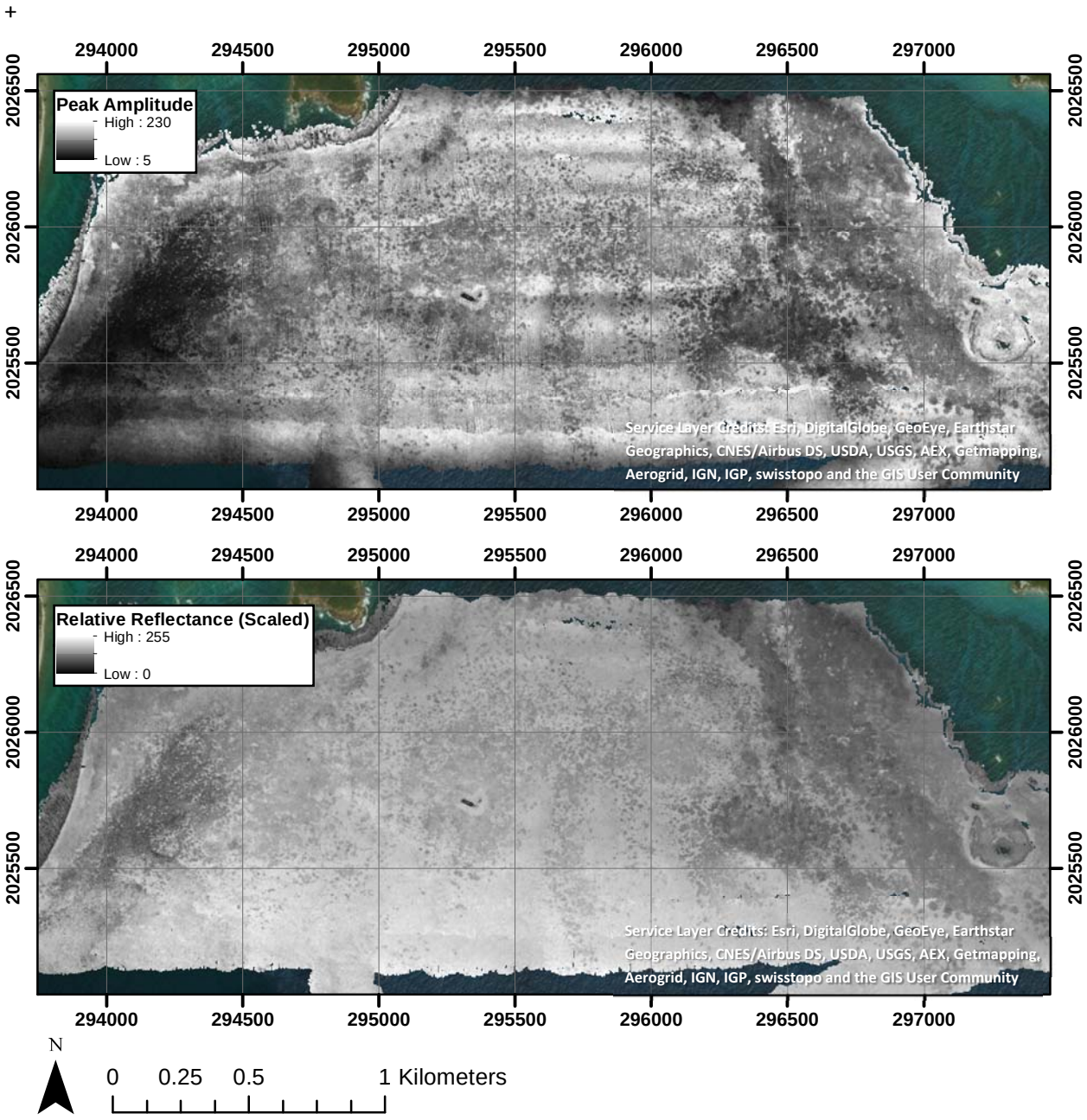

Figure 4-8: Peak bottom return amplitude (top) and relative reflectance (bottom) generated from deep channel data.

Figure 4-9 shows a region in which seafloor textures can be distinguished in relative reflectance products that had previously been obscured due to depth artifacts.

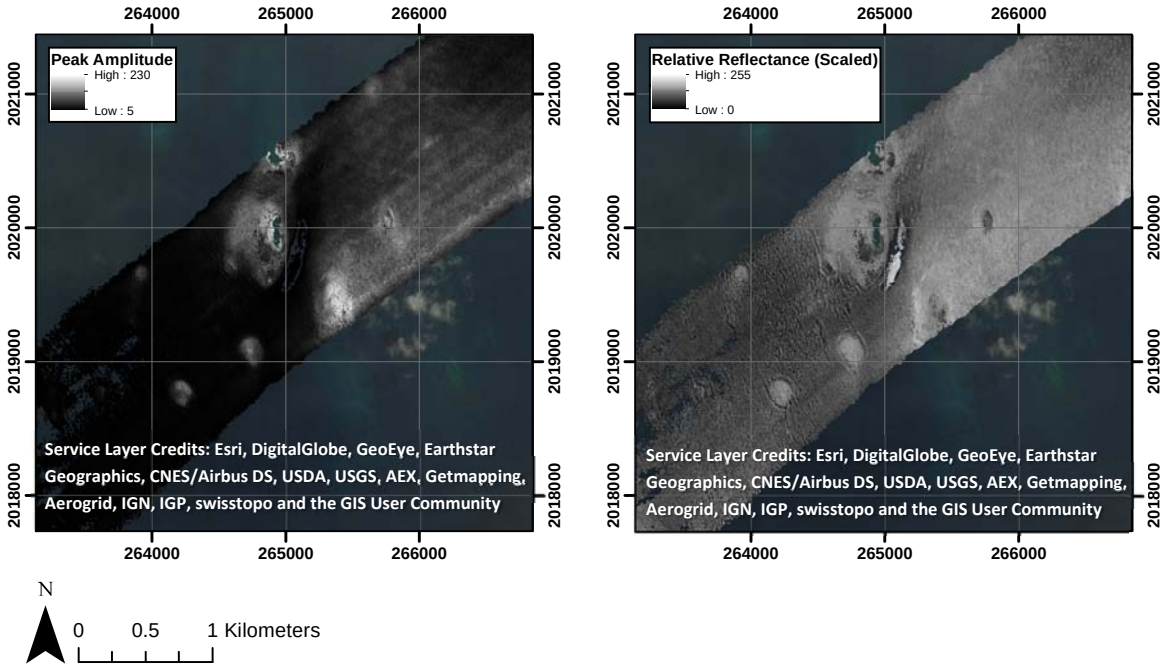

Figure 4-9: Seafloor textures visible in relative reflectance products (right) which are not distinguishable in uncorrected peak bottom return products (left).

Figure 4-10 shows a region in which angle of incidence artifacts are still present in final relative reflectance products. The rate at which intensity falls off relative to incidence angle is a function of how specular the bottom type is. Because correction parameters are determined from trends in the data, regions like this where corrections have been either overapplied, or underapplied, remain in the final product.

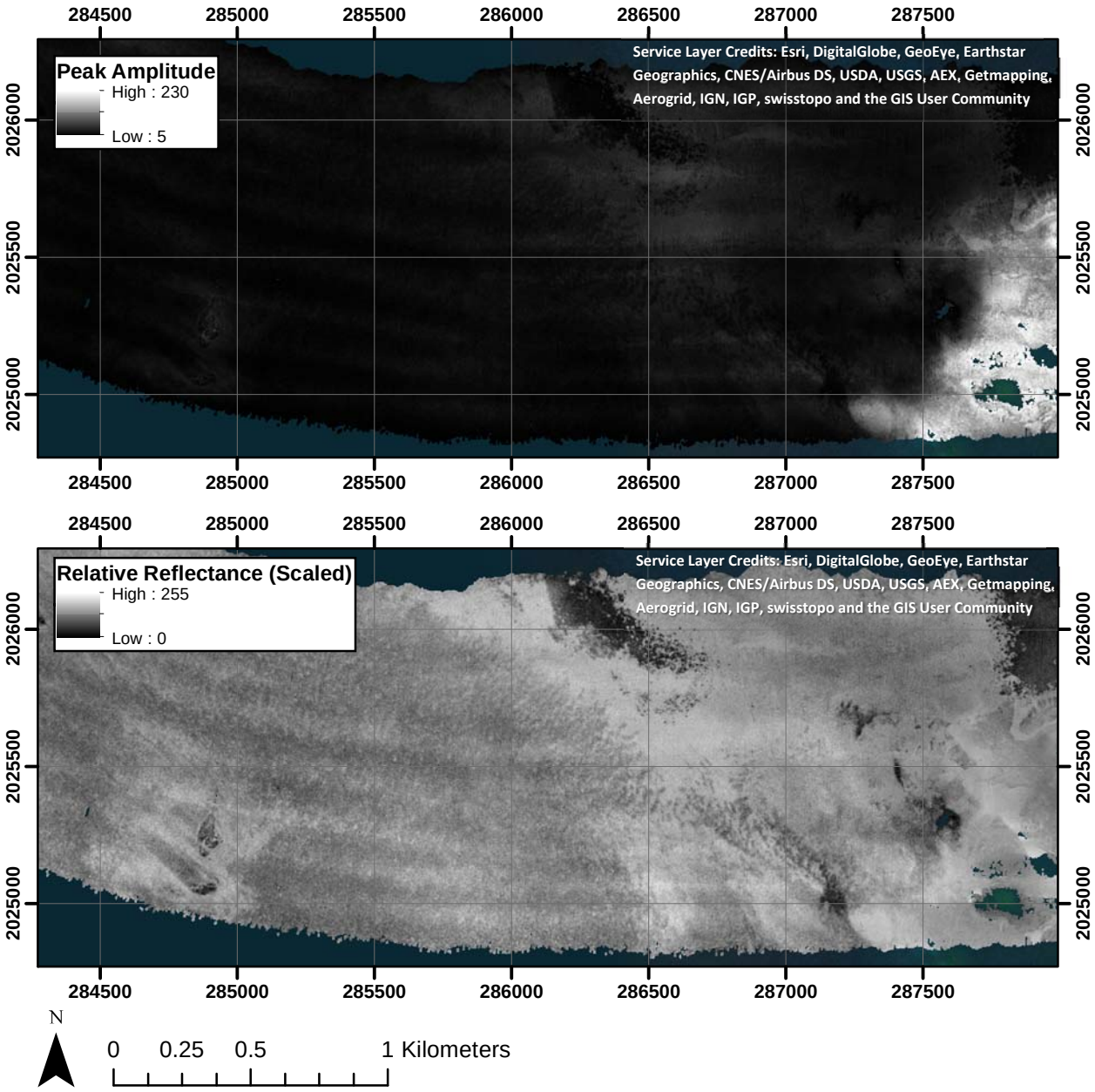

Figure 4-10: Some seamline artifacts remain in final relative reflectance products (bottom), though these are more localized relative to raw peak bottom return products (top)

4.3.5 Quantitative Assessment

In July of 2012, seafloor reflectance spectra measurements, measured at 532 nm, were collected using an Ocean Optics USB2000 spectrometer as part of a field validation of the EAARL-B. The method used to collect these seafloor spectra is described in Pe'eri et al. (2013). Briefly, the method consisted of

mounting the spectrometer probe to an underwater camera frame, which could be lowered from the deck of a small boat (Figure 4-11).

Figure 4-11: Equipment used for obtaining seafloor reflectance spectra (shown operated by Stephen White of NOAA's National Geodetic Survey, Remote Sensing Division).

The spectrometer probe was connected to the instrument on the boat by a 25-m fiber optic cable. Additionally, a white reference panel, controlled by a pneumatic actuator, was used to obtain reference spectra to normalize the seafloor spectra, correcting for variable downwelling irradiance. Temporal changes in benthic habitat boundaries during the two year span between data collections limited the applicability of the control spectra measurements. Prior to conducting quantitative assessment, historic Google Earth imagery was used to reject control spectra values that were either (1) within a region in which the bottom type has changed, or (2) over a region between two adjacent bottom types. Figure 4-12 shows reference spectra location used as a part of this assessment.

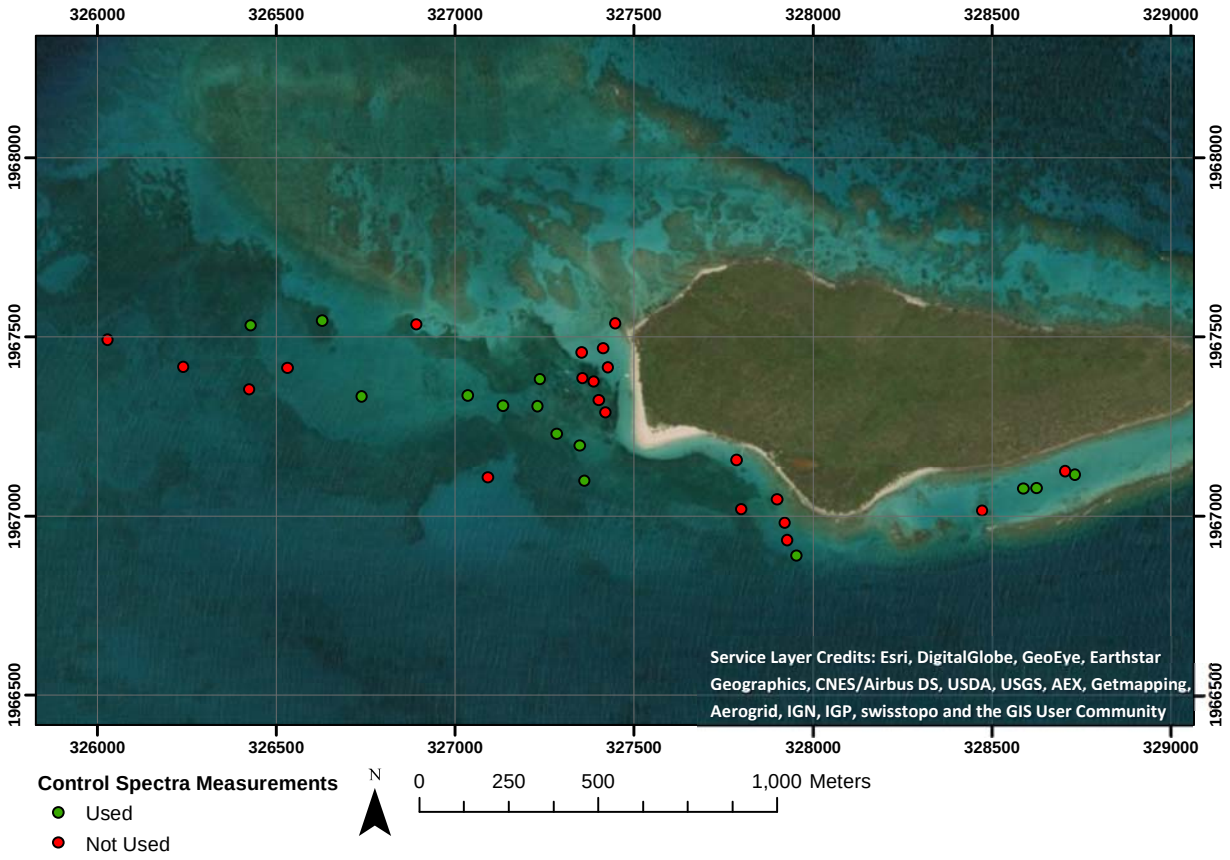

Figure 4-12: Control spectra measurements acquired in 2012 and used as a part of quantitative assessment.

The remaining points were used as control measurements in order to quantify the improvement in the correlation of relative reflectance products to true reflectance, comparatively to the uncorrected peak bottom return amplitude values collected with the EAARL-B. Reference spectra measurements were collected up to approximately 10 meters, limiting their use utility as control reflectance values to data collected with the EAARL-B shallow depth receiver channel.

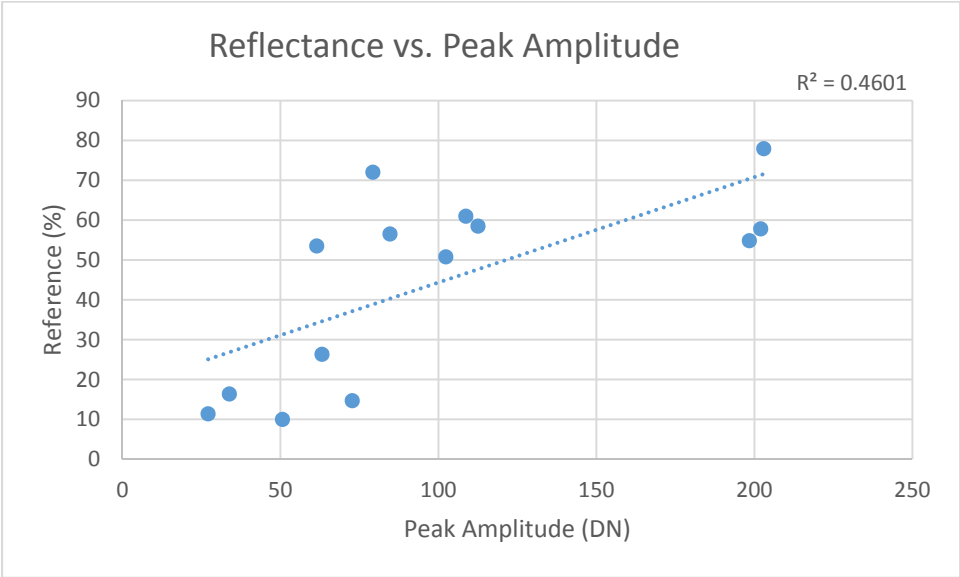

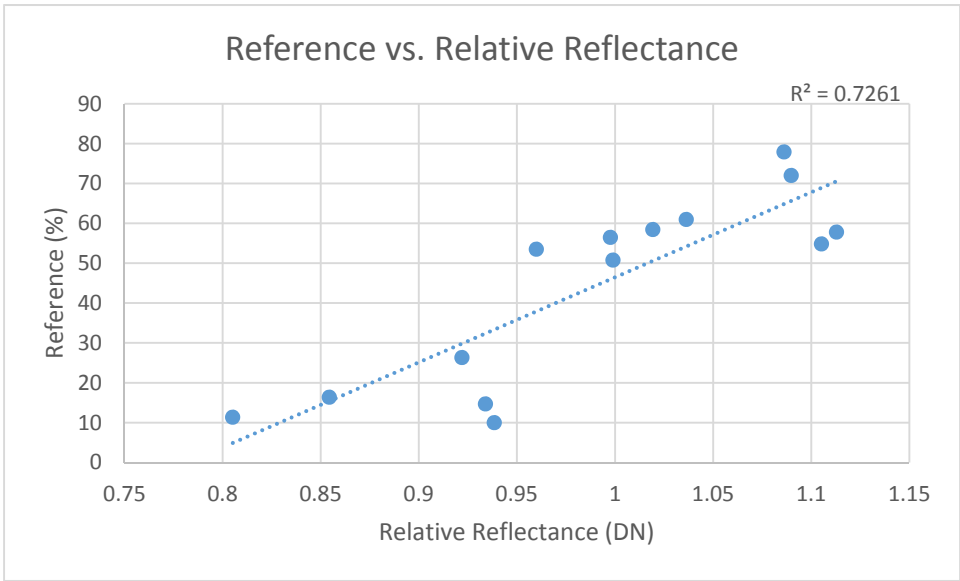

Figure 4-13: Bottom return peak amplitude and relative reflectance regressed against reference spectra measurements with associated R^2 values.

The regressions shown in Figure 4-13 show an improvement in R^2 value from 0.46 to 0.73. This increase in R^2 indicates an improvement in how well relative reflectance products relate to true seafloor bottom reflectance compared to peak bottom return amplitude. It is reasonable to assume the fit would have been even better, if not for the two-year time span between the reference data acquisition and EAARL-B overflights, during which time seagrass density changed quite significantly, as noted in Google Earth imagery.

5. CONCLUSIONS

Bathymetric lidar has already been well established as a useful tool for benthic habitat mapping, enabling efficient data acquisition in shallow to moderate depth ranges, including many of the coral reef habitats mapped and monitored by NOAA's Center for Coastal Monitoring and Assessment (CCMA). Previous research has documented the ability to supplement lidar bathymetry and enhance its utility for benthic habitat mapping through the generation of additional data products (beyond bathymetric surfaces) from return lidar waveforms. Notable examples of such products include seafloor relative reflectance mosaics, which can be produced by applying corrections to bottom return "intensity" data, and are already in fairly widespread use by CCMA and others for seafloor habitat mapping.

The USGS EAARL-B system, which was used to acquire data in priority USVI coral reef habitat areas for NOAA CCMA in 2014, features a novel design and provides a number of performance enhancements over the original EAARL system. However, like its predecessor, the EAARL-B lacked functionality for generating seafloor relative reflectance products. Furthermore, the EAARL-B's unique design characteristics, including its scan pattern, were considered to impose some challenges for relative reflectance mapping. This research has taken significant steps to address these challenges through development and testing of new algorithms and procedures for generating relative reflectance mosaics from EAARL-B data. The procedures were first developed and evaluated using data acquired in Barnegat Bay, New Jersey, and Buck Island, St. Croix, USVI and then extended to a much larger project site south of St. Thomas, USVI. Detailed analysis of the results confirms that the EAARL-B can be effectively used for seafloor relative reflectance mapping, one of the primary findings of this research. Visual, qualitative analysis of the outputs indicates that seamlines and other salient artifacts have been largely eliminated, and quantitative comparison of data in areas of swath overlap (including data from multiple days' flights) confirms that the confounding effects of variable depth and incidence angle have been greatly reduced through the processing procedures developed in this work. The algorithms and procedures are being provided to NOAA to enable relative reflectance mosaics to be generated for all future projects involving data acquisition with the EAARL-B and/or similar topographic-bathymetric lidar systems.

Another contribution of this work was the development of procedures for generating additional waveform-shape based features from EAARL-B data. These features include grids generated from bottom return peak amplitude, skewness, and area under the curve. Waveform feature grids were generated for a subset of the St. Thomas EAARL-B data covering Flat Cays, south of Charlotte Amalie.

The same corrections developed for the relative reflectance products—namely, depth and incidence angle—were adapted to these additional waveform features. Although these new products have only been visually assessed to date, they appear to contain additional information (beyond depth and relative reflectance) that may be helpful in seafloor characterization.

Next steps in our long-range research program will include work to be led by project partners in CCMA's Biogeography Branch and at the University of New Hampshire Center for Coastal and Ocean Mapping – Joint Hydrographic Center (CCOM-JHC). The USVI relative reflectance mosaics will be integrated with existing data by CCMA and used to update USVI benthic habitat maps. Additionally, the waveform features for Flat Cays will be evaluated for seascape habitat complexity and composition analysis that extends beyond current habitat mapping capabilities. For example, these additional waveform feature products may prove useful in predicting species richness, canopy cover, coral heights, coral health and other biophysical parameters of interest to NOAA. It is anticipated that this additional information will contribute to management of coral reef ecosystems. These capabilities will be evaluated by the NOAA-UNH-OSU project team using field data (underwater video and diver observations) collected by NOAA in September of 2016 for the Flat Cays region.

This research has also led to a number of recommendations for follow-on studies. To facilitate further quantitative assessment of the reflectance products, it is recommended underwater spectra, collected with an Analytical Spectral Devices (ASD) DiveSpec or Ocean Optics spectrometer following procedures of Pe'eri et al. (2013), be obtained concurrently with lidar acquisition. Additionally, it is recommended that the underwater reflectance spectra be collected in deeper waters, if feasible, such that relative reflectance from the deep water receiver channel can also be quantitatively assessed. Another interesting finding of this work is the effect of ambient sunlight (especially, sun glint) on relative reflectance and other waveform-derived products. It is highly recommended that these effects be further quantified in future work, such that additional corrections can be applied. To the knowledge of the project team, such corrections have not previously been developed for bathymetric lidar relative reflectance data, yet the effects of sunlight were clearly identifiable in our results. Yet another suggested enhancement to the methods developed in this research is to eliminate the simplifying assumption of a flat seafloor, which is used in the incidence correction. Specifically, elevation values of points could be used to approximate surface normals, and provide a better angle of incidence correction in areas of large relief.

WORKS CITED

Brown, C. J., Smith, S. J., Lawton, P., & Anderson, J. T. (2011). Benthic habitat mapping: a review of progress towards improved understanding of the spatial ecology of the seafloor using acoustic techniques. *Estuarine, Coastal and Shelf Science, 92*(3), 502-520.

Carr, D., & Tuell, G. (2014). Estimating field-of-view loss in bathymetric lidar: application to large-scale simulations. *Applied optics*, *53*(21), 4716-4721.

Catanzaro, D., Rogers, C.S., HIllis-Starr, Z., Nemeth, R.S., & Taylor, M. (2002). Status of Coral Reefs of the U.S. Virgin Islands. In: D.D. Turgeon, R.G. Asch, B.D. Causey, R.E. Dodge, W. Jaap, K. Banks, J. Delaney, B.D. Keller, R. Speiler, C.A. Mato, J.R.Garcia, E. Diaz, D. Catanzaro, C.S. Rogers, Z. Hillis-Starr, R.S. Nemeth, M. Taylor, G.P. Schmahl, M.W. Miller, D.A. Gulko, J.E. Maragos, A. Friedlander, C.L. Hunter, R.S. Brainard, R. Craig, R.H. Richmond, G. Davis, J. Starmer, M. Trianni, R. Houk, C.E. Birkeland, A. dward, Y. Golbuu, J. Gutierrez, N. Idechong, G. Paulay, A. Tafileichig, & N.V. Velde (Eds.). *The State of Coral Reef Ecosystems of the United States and Pacific Freely Associated States: 2002* (pp. 131-150). Silver Spring, MD: NOAA/NOS/NCCOS.

Collin, A., Archambault, P., & Long, B. (2008). Mapping the shallow water seabed habitat with the SHOALS. *IEEE Transactions on Geoscience and Remote Sensing*, *46*(10), 2947-2955.

Collin, A., Archambault, P., & Long, B. (2011). Predicting species diversity of benthic communities within turbid nearshore using full-waveform bathymetric LiDAR and machine learners. *PloS one*, *6*(6), e21265.

Collin, A., Long, B., & Archambault, P. (2012). Merging land-marine realms: Spatial patterns of seamless coastal habitats using a multispectral LiDAR. *Remote Sensing of Environment*, *123*, 390-399.

Costa, B. M., Battista, T. A., & Pittman, S. J. (2009 (a)). Comparative evaluation of airborne LiDAR and ship-based multibeam SoNAR bathymetry and intensity for mapping coral reef ecosystems. *Remote Sensing of Environment*, *113*(5), 1082-1100.

Costa, B.M., Bauer, L.J., Battista, T.A., Mueller, P.W., & Monaco, M.E. (2009 (b)). *Moderate-Depth Benthic Habitats of St. John, U.S. Virgin Islands*. NOAA Technical Memorandum NOS NCCOS 105. Silver Spring, MD.

Costa, B.M., Tormey, S., & Battista, T.A. (2012). *Benthic Habitats of Buck Island Reef National Monument*. NOAA Technical Memorandum NOS NCCOS 142. Prepared by the NCCOS Center for Coastal Monitoring and Assessment Biogeography Branch. Silver Spring, MD.

Costa, B., Battista, T., Parrish, C., & Wilson, N. (2016). Evaluating the Utility of EAARL-B Lidar Waveforms for Mapping Coral Reef Habitats presented at the 17th Annual Coastal Mapping & Charting Workshop of the Joint Airborne Lidar Bathymetry Technical Center of Expertise (JALBTCX), July 19-21, 2016. Silver Spring, MD.

Feygels, V. I., Wright, C. W., Kopilevich, Y. I., & Surkov, A. I. (2003 (a)). Narrow-field-of-view bathymetrical lidar: theory and field test. *Proc. SPIE, Vol. 2694,* 1-11.

Feygels, V.I., Kopelevich, Y.I., Surkov, A.I., Yungel, J.K., Behrenfeld, M.J. (2003 (b)). Airborne lidar system with variable field of view receiver for water optical properties measurement. *Proc. SPIE, Vol. 5155*, 12-21.

Fischler, M. A., & Bolles, R. C. (1981). Random sample consensus: a paradigm for model fitting with applications to image analysis and automated cartography. *Communications of the ACM, 24*(6), 381-395.

Fredericks, Xan, Kranenburg, C.J., Nagle, D.B. (2015). EAARL-B Submerged Topography—Saint Thomas, U.S. Virgin Islands, 2014: U.S. Geological Survey data release, http://dx.doi.org/10.5066/F7G15XXG.

Guenther, G.C. (1985). Airborne laser hydrography: System design and performance factors, *NOAA Professional Paper Series*, National Ocean Service 1, National Oceanic and Atmospheric Administration, Rockville, MD, 385 pp.

Guenther, G. C., Thomas, R. W. L., & LaRocque, P. E. (1996). Design considerations for achieving high accuracy with the SHOALS bathymetric lidar system. *Proc. SPIE, Vol. 2964,* 2–25.

Guenther, G. C., Cunningham, A. G., LaRocque, P. E., & Reid, D. J. (2000). Meeting the accuracy challenge in Airborne Lidar Bathymetry. *Proc. EARSeL-SIG-Workshop LIDAR, Dresden/FRG.*

Guenther, G.C. (2007) Chaper 8: Airborne LIDAR Bathymetry. In D.F. Maune (Ed.), *Digital Elevation Model Technologies and Applications: The Dem User's Manual, 2nd Edition.* (pp. 253-320). Bethesda, MD: American Society for Photogrammetry and Remote Sensing.

Heidemann, H.K., Stoker, J., Brown, D., Olsen, M.J., Singh, R., Williams, K., Chin, A., Karlin, A., McClung, G., Janke, J., Shan, J., Kim, K.H., Sampath, A., Ural, S., Parrish,C.E., Waters, K., Wozencraft, J., Macon, C.L., Brock, J., Wright, C.W., Hopkinson, C., Pietroniro, A., Madin, I., & Conner, J. (2012). Chapter 10: Applications. In M. Renslow (Ed.), *Manual of Airborne Topographic Lidar.* (pp. 253-320). Bethesda, MD: American Society for Photogrammetry and Remote Sensing.

Jeffrey, C.F.G., Anlauf, U., Beets, J., Caseau, S., Coles, W., Friedlander, A., Herzlieb, S., Hillis-Starr, Z., Kendall, M., Mayor, V., Miller, J., Nemeth, R.S., Rogers, C.S., & Toller, W. (2005). Chapther 2: The State of Coral Reef Ecosystems of the U.S. Virgin Islands. In J.E. Waddell (Ed.), *The State of Coral Reef Ecosystems of the United States and Pacific Freely Associated States: 2005* (pp. 45-88). NOAA Technical Memorandum NOS NCCOS 11. Silver Spring, MD.

Jutzi, B., & Gross, H. (2009). Normalization of LiDAR intensity data based on range and surface incidence angle. *Proc. IAPRS, 38*, 213-218.

Kashani, A. G., Olsen, M. J., Parrish, C. E., & Wilson, N. (2015). A review of LIDAR radiometric processing: from Ad Hoc intensity correction to rigorous radiometric calibration. *Sensors*, *15*(11), 28099-28128.

Kendall, M.S., Monaco, M.E., Buja, K.R., Christensen, J.D., Kruer, C.R., Finkbeiner, M., & Warner, R.A. (2001). *Methods Used to Map the Benthic Habitats of Puerto Rico and the U.S. Virgin Islands.* NOAA Technical Memorandum NOAA NCCOS CCMA 152. Silver Spring, MD.

Kinney, J., Bogonko, M., White, M., Armstrong, A., Nagel, E., Dijkstra, J., Parrish, C., & Wilson, N. (2016). Intensity and Reflectance for Habitat Mapping and Seafloor Characterization using the Superstorm Sandy Lidar Data. The 17th Annual Coastal Mapping & Charting Workshop of the Joint Airborne Lidar Bathymetry Technical Center of Expertise (JALBTCX), July 19-21, 2016. Silver Spring, MD.

Lee, M. (2003). *Benthic Mapping of Coastal Waters Using Data Fusion of Hyperspectral Imagery and Airborne Laser Bathymetry* (Doctoral Dissertation). Retrieved from http://etd.fcla.edu/UF/UFE0000730/lee_m.pdf.

Long, B., Aucoin, F., Montreuil, S., Robitaille, V., & Xhardé, R. (2010). Airborne LIDAR bathymetry applied to coastal hydrodynamic processes. *Coastal Engineering Proceedings*, *1*(32), 26.

Macon, C., Wozencraft, J., Park, J.Y., & Tuell, G. (2008). Seafloor and land cover classification through airborne LIDAR and hyperspectral data fusion. *Proc. of the 2008 IEEE International Geoscience and Remote Sensing Symposium, 2*, July 7-11, 2008. Boston, MA.

Monaco, M.E., Anderson, S.M., Battista, T.A., Kendall, M.S., Rohmann, S.O., Wedding, L.M., & Clarke, A.M. (2012). *National Summary of NOAA's Shallow-water Benthic Habitat Mapping of U.S. Coral Reef Ecosystems*. NOAA Technical Memorandum NOS NCCOS 122. Silver Spring, MD.

Mumby, P. J., & Harborne, A. R. (1999). Development of a systematic classification scheme of marine habitats to facilitate regional management and mapping of Caribbean coral reefs. *Biological conservation*, *88*(2), 155-163.

Nagle, D. B., & Wright, C.W. (2016). *Algorithms used in the Airborne Lidar Processing System (ALPS): U.S. Geological Survey Open-File Report 2016–1046.* http://dx.doi.org/10.3133/20161046.

Narayanan, R., Kim, H. B., & Sohn, G. (2009). Classification of SHOALS 3000 bathymetric LIDAR signals using decision tree and ensemble techniques. *IEEE TIC-STH,* 462-467.

Parrish, C.E., Jeong, I., Nowak, R.D., & Brent Smith, R. (2011). Empirical comparison of full-waveform lidar algorithms: Range extraction and discrimination performance. *Photogrammetric Engineering & Remote Sensing*, *77*(8), 825-838.

Parrish, C.E., Rogers, J.N., & Calder, B.R. (2014). Assessment of waveform features for lidar uncertainty modeling in a coastal salt marsh environment. *IEEE Geoscience and Remote Sensing Letters*, *11*(2), 569-573.

Parrish, C.E. & Wilson, N., (2015). Topobathymetric Lidar Waveform Features for Habitat Mapping and Hurricane Sandy Response. The 16th Annual Coastal Mapping & Charting Workshop of the Joint Airborne Lidar Bathymetry Technical Center of Expertise (JALBTCX), June 16-18, 2015. Corvallis, OR.

Parrish, C.E., Forfinski, N., & Wilson, N. (2016 (a)). Advances in Seafloor Mapping with New Spaceborne and Airborne Lidar Systems. The 17th Annual Coastal Mapping & Charting Workshop of the Joint Airborne Lidar Bathymetry Technical Center of Expertise (JALBTCX), July 19-21, 2016. Silver Spring, MD.

Parrish, C.E., Dijkstra, J.A., O'Neil-Dunne, J.P., McKenna, L., & Pe'eri, S., 2016 (b). Post-Sandy Benthic Habitat Mapping Using New Topobathymetric Lidar Technology and Object-Based Image Classification. *Journal of Coastal Research*, *76*(sp1), 200-208.

Pe'eri, S., McLeod, A., Lavoie, P., Ackerman, S., Gardner, J., & Parrish, C. (2013). Field calibration and validation of remote-sensing surveys. *International journal of remote sensing*, *34*(18), 6423-6436.

Phong, B. T. (1975). Illumination for computer generated pictures. *Communications of the ACM*, *18*(6), 311-317.

Pittman, S. J., & Brown, K. A. (2011). Multi-scale approach for predicting fish species distributions across coral reef seascapes. *PloS one*, *6*(5): e20583.

Quadros, N. D. (2013). Unlocking the characteristics of Bathymetric Lidar sensors. *LiDAR Magazine*, *3*, 62-67.

Rogers, J. N., Parrish, C. E., Ward, L. G., & Burdick, D. M. (2015). Evaluation of field-measured vertical obscuration and full waveform lidar to assess salt marsh vegetation biophysical parameters. *Remote Sensing of Environment*, *156*, 264-275.

Rothenberger P., Blondeau J., Cox C., Curtis S., Fisher W.S., Garrison V., Hillis-Starr Z., Jeffrey C.F., Kadison E., Lundgren I., & Miller W.J. (2008). Chapter 2: The state of coral reef ecosystems of the U.S. Virgin Islands. In J.E. Waddell & A.M. Clarke (Eds.), *The state of coral reef ecosystems of the United States and Pacific Freely Associated States: 2008* (pp. 29-73). NOAA Technical Memorandum NOS NCCOS 73. Silver Spring, MD.

Steinvall, O. & Koppari, K. (1996). Depth sounding lidar: An overview of Swedish activities and future prospects. *Proc. SPIE, Vol. 2964*, 2-25.

Tuell, G., Park, J.Y., Aitken, J., Ramnath, V., Feygels, V., Guenther, G., & Kopilevich, Y. (2005) SHOALS-enabled 3D benthic mapping. *Proc. SPIE Vol. 5806,* 816-826.

Tuell, G.H., Feygels, V., Kopilevich, Y., Weidemann, A.D., Cunningham, A.G., Mani, R., Podoba, V., Park, J.Y., & Aitken, J. (2005). Measurement of ocean water optical properties and seafloor reflectance with scanning hydrographic operational airborne lidar survey (SHOALS): II. Practical results and comparison with independent data. *Proc. SPIE Vol. 5885,* 58850E-1-58850E-13.

Tuell, G. H., Park, J. Y., Aitken, J., Ramnath, V., Feygels, V., & Kopelivich, Y. (2005). Fusion of SHOALS bathymetric lidar and passive spectral data for shallow water rapid environmental assessment. *Europe Oceans 2005*, 2, 1046–1051. http://doi.org/10.1109/OCEANSE.2005.1513202

Tuell, G., & Carr, D. (2013). New Procedure for Estimating Field-of-View Loss in Bathymetric LIDAR. *Imaging and Applied Optics,* OSA Technical Digest. Paper ITh3D.4.

Wang, C. K., & Philpot, W. D. (2002). Using SHOALS LIDAR system to detect bottom material change. *IEEE International Geoscience and Remote Sensing Symposium, 5*, 2690-2692.

Wang, C. K., & Philpot, W. D. (2007). Using airborne bathymetric lidar to detect bottom type variation in shallow waters. *Remote Sensing of Environment*, *106*(1), 123-135.

Wright, C.W. (2014). USGS EAARL-B: Missions, Calibration & Validation. 15th Annual Coastal Mapping & Charting Workshop of the Joint Airborne Lidar Bathymetry Technical Center of Expertise (JALBTCX), June 10-12, 2014. Mobile, AL.

Wright, C.W., Kranenburg, C., Battista, T.A., & Parrish, C. (2016). Depth Calibration and Validation of the Experimental Advanced Airborne Research Lidar, EAARL-B. *Journal of Coastal Research*, *76*(sp1), 4-17.

Wright, C.W., Kranenburg, C.J., Troche, R.J., Mitchell, R.W., and, Nagle, D.B. (2016). Depth calibration of the experimental advanced airborne research lidar, EAARL-B. *U.S. Geological Survey Open-File Report 2016–1048*. http://dx.doi.org/10.3133/ofr20161048.

Zitello, A.G., Bauer, L.J., Battista, T.A., Mueller, P.W., Kendall M.S. & Monaco, M.E. (2009). *Shallow-Water Benthic Habitats of St. John, U.S. Virgin Islands*. NOAA Technical Memorandum NOS NCCOS 96. Silver Spring, MD.

APPENDIX

Relative reflectance MATLAB scripts

Correction function:

```
function [] =
correct_bottom_intensity_deep(inputFile,outputFile,skipRow,downsampleInt)

%%%%%%%%%%%%%%%%%%%%%%%%%%%%%%%%%%%%%%%%%%%%%%%%%%%%%%%%%%%%%%%%%%%%%%%%%%%%%%%%
%  correct_bottom_intensity_deep                                                 %
%                                                                                %
%  This program applies two correctons to EAARL-B "bottom intensity"             %
%  (i.e., bottom return peak amplitude): 1) a depth correction and 2) an         %
%  incidence angle correction.                                                   %
%  After corrrections are applied, a rough outlier removal is applied,           %
%  removing all points greater than 3 standard deviations away from the          %
%  mean. Final corrected values are scaled to 0-255. This script is the          %
%  same as correct_bottom_intensity_shallow, but with a filter to remove         %
%  saturated points.                                                             %
%                                                                                %
%  Adjustable Parameters:                                                        %
%    inputFile = the directory conpaining EAARL-B waveform features files.%
%                The expected format of each file is comma-delimited             %
%                with the following fields: x,y,z,depth,skew,auc,                %
%                stdev,peak,soe,raster,channel,pulse,aoi,aoih,aoiv               %
%    outputFile = the directory in which files containing x,y,elev,depth,        %
%                peak_raw,depth_corrected,aoi_corrected will be stored           %
%    skipRow = amount of rows to skip when reading files, set as                 %
%                1 if there is a single line header.                             %
%    downsampleInt = integer value to downsample input file for                  %
%                correction determination. Every nth sample starting with%
%                the first sample is kept. This is only for determination%
%                of correction values, output will include full data set.%
%                Set to 1 to use all samples.                                    %
%                                                                                %
%  N. Wilson, email: wilsonn2@oregonstate.edu                                    %
%  C. Parrish, email: Christopher.Parrish@oregonstate.edu                        %
%  Created:  7/10/2015                                                           %
%  Modified: 1/19/2017                                                           %
%%%%%%%%%%%%%%%%%%%%%%%%%%%%%%%%%%%%%%%%%%%%%%%%%%%%%%%%%%%%%%%%%%%%%%%%%%%%%%%%
format long g


%% Read the EAARL-B waveform features file

M = dlmread(inputFile, ',', skipRow, 0);

% remove saturated points, points with intensity greater than 230 or at
% less than 10 meters depth.
indx_remove = M(:,8) ==0 | M(:,8)>230 |  M(:,4) < 10;
M(indx_remove,:) = []; % remove these array elements
```

```
Mdownsample = downsample(M,downsampleInt);

% Downsample these fields to make correction derivation faster
depth= Mdownsample(:,4);
peak= Mdownsample(:,8);
aoih= Mdownsample(:,14);
peak_log = log(peak);
slope_dist = depth ./ cosd(aoih);


depthAll= M(:,4);
peakAll= M(:,8);
aoihAll= M(:,14);
peak_log_all = log(peakAll);
slope_dist_all = depthAll ./ cosd(aoihAll);

%% Depth Correction
% Limit coefficient derivation values to prevent outliers from taking over
mval1 = mean(peak_log);
sval1 = std(peak_log);
limVal1 = mval1 + 2*sval1;
indx = peak_log<limVal1;

[~,fitresult1,gof_depth] = depth_correct(slope_dist(indx),peak_log(indx));

coeffs = coeffvalues(fitresult1);

a = coeffs(1);
b = coeffs(2);

%% Apply the depth correction.
IntCorr1 = peak_log./(a.*slope_dist +b);
IntCorr1_all = peak_log_all./(a.*slope_dist_all +b);

%% Determine angle of incidence correction
[~,fitresult2,gof_aoi] = aoi_correct(aoih(indx),IntCorr1(indx));

coeffsAOI = coeffvalues(fitresult2);

aAOI = coeffsAOI(1);
bAOI = coeffsAOI(2);

%% Apply the angle of incidence correction
IntCorr2_all = IntCorr1_all./(aAOI.*cosd(aoihAll).^(bAOI));

%% Remove outliers that are greater than 3 standard devations away from mean
stdDev = std(IntCorr2_all);
average = mean(IntCorr2_all);
upperLim = average + 3*stdDev;
lowerLim = average - 3*stdDev;

I = find(IntCorr2_all>upperLim | IntCorr2_all < lowerLim);
```

```
M(I,:) = []; % remove these array elements

IntCorr1_all(I)= [];
IntCorr2_all(I)= [];

eastingAll = M(:,1);
northingAll = M(:,2);
elevAll = M(:,3);
depthAll= M(:,4);
peakAll= M(:,8);
soeAll= M(:,9);


%% Scale values to 0-255
[depth_corrected] = scale_min_max_f(IntCorr1_all);

[aoi_corrected] = scale_min_max_f(IntCorr2_all);

%% Write values to output file

title = 'x,y,elev,depth,soe,peak_raw,depth_corrected,aoi_corrected';
write_vals = [eastingAll northingAll elevAll depthAll soeAll peakAll
depth_corrected aoi_corrected];
fileID = fopen(outputFile,'w');
fprintf(fileID,'%s\n',title);
fprintf(fileID,'%.2f,%.2f,%.2f,%.2f,%.4f,%.2f,%.2f,%.2f\n',write_vals');
fclose(fileID);

disp('Done--the file with corrected bottom intensities has been created!')
```

Depth correction function:

```
function [peak_corrected,fitresult,gof] = depth_correct(depth,peak)

[xData, yData] = prepareCurveData( depth, peak );

% Set up fittype and options.
ft = fittype( 'poly1' );

% Fit model to data.
[fitresult, gof] = fit( xData, yData, ft );

coeffs = coeffvalues(fitresult);

a = coeffs(1);
b = coeffs(2);

%% Apply the depth correction.
peak_corrected = peak./(a.*depth +b);
```

Incidence angle correction function:

```
 function [peak_corrected,fitresult,gof] = aoi_correct(aoi,peak)

[xData, yData] = prepareCurveData( aoi, peak );

% Set up fittype and options.
ft = fittype( 'a*cosd(x)^(b)', 'independent', 'x', 'dependent', 'z' );
opts = fitoptions( 'Method', 'NonlinearLeastSquares' );
opts.Display = 'Off';
opts.StartPoint = [0.381558457093008 0];

% Fit model to data.
[fitresult, gof] = fit( xData, yData, ft, opts );

coeffsAOI = coeffvalues(fitresult);

aAOI = coeffsAOI(1);
bAOI = coeffsAOI(2);

%% Apply the angle of incidence correction
peak_corrected = peak./(aAOI.*cosd(aoi).^(bAOI));
```

Normalization function:

```
function [val1_norm] = normalize_f(x1,y1,r1,x2,y2,r2)

%%%%%%%%%%%%%%%%%%%%%%%%%%%%%%%%%%%%%%%%%%%%%%%%%%%%%%%%%%%%%%%%%%%%%%%%%%%%%%%
%  normalize_f                                                                  %
%                                                                               %
%  Function to normalize points from overlapping datasets. r1 values are       %
%  adjusted so that the mean and standard deviation match with r2.              %
%  val1_norm are normalized r1 values. Only points within 1 meter of            %
%  eachother are used for normalization.                                        %
%                                                                               %
%  N. Wilson, email: wilsonn2@oregonstate.edu                                   %
%  Created:  01/03/2017                                                         %
%%%%%%%%%%%%%%%%%%%%%%%%%%%%%%%%%%%%%%%%%%%%%%%%%%%%%%%%%%%%%%%%%%%%%%%%%%%%%%%

coords1 = [x1 y1];

coords2 = [x2 y2];

% k is the closest point in X for each point in XI. d is the distance beween
% those points.

[k,d] = knnsearch(coords1,coords2);

% all points within 1 meter of another
indx = d<1;
```

```
val1 = r1(k(indx),:);
val2 = r2(indx,:);

% At these indices calculate the difference in intensity values
sigmaRef = std(val2);
sigmaAdjust = std(val1);

muRef = mean(val2);
muAdjust = mean(val1);

r1_normalized2 = (sigmaRef/sigmaAdjust)*(r1 - muAdjust) + muRef;

val1_norm =  (sigmaRef/sigmaAdjust)*(r1 - muAdjust) + muRef;


disp('Done!')
```